PSFC/RR-10-4

An Assessment of the Current Data Affecting Tritium Retention and its Use to Project Towards T Retention in ITER

Lipschultz, B.[1], Roth, J.[2], Davis, J.W.[3], Doerner, R.P.[4],
Haasz, A.A.[3], Kalenbach, A.[2], Kirschner, A.[5],
Kolasinski, R.D.[6], Loarte, A.[7], Philipps, V.[5],
Schmid, K.[2], Wampler, W.R.[8],
Wright, G.M.[9], Whyte, D.G.[1]

April 2010

Plasma Science and Fusion Center
Massachusetts Institute of Technology
Cambridge MA 02139 USA

[1]MIT Plasma Science & Fusion Center, Cambridge, MA 02139, USA
[2]Max-Planck Institut für Plasmaphysik, Boltzmannstraße 2, 85748 Garching, Germany
[3]U. of Toronto Institute for Aerospace Studies, 4925 Dufferin St, Toronto, ON, M3H5T6, Canada
[4]U.C.S.D. Center for Energy Research 9500 Gilman Dr. La Jolla, CA. 92093, USA
[5]Forschungszentrum Jülich, 52425 Jülich, Germany
[6]Sandia Laboratories, P.O. Box 969 / MS 9161, Livermore, CA, 94550-9610, USA
[7]ITER ORG. Fusion Science and Technology Dept., Cadarache - Building 523 13108 St. Paul-lez-Durance, France
[8]Sandia Laboratories, Org. 1111, MS 1056 Albuquerque NM 87185, USA
[9]FOM-Rijnhuizen, Postbus 1207, NL-3430 BE, Nieuwegein, The Netherlands

The work of the MIT authors was supported by the U.S. Department of Energy, Grant No. DE-FC02-99ER54512.

An assessment of the current data affecting tritium retention and its use to project towards T retention in ITER

B. Lipschultz[1], J. Roth[2], J.W. Davis[3], R.P. Doerner[4], A.A. Haasz[3], A. Kallenbach[2], A. Kirschner[5], R.D. Kolasinski[6], A. Loarte[7], V. Philipps[5], K. Schmid[2], W.R. Wampler[8], G.M. Wright[9], D.G. Whyte[1]

[1]MIT Plasma Science & Fusion Center, Cambridge, MA 02139, USA
[2]Max-Planck Institut für Plasmaphysik, Boltzmannstraße 2, 85748 Garching, Germany
[3]U. of Toronto Institute for Aerospace Studies, 4925 Dufferin St, Toronto, ON, M3H5T6, Canada
[4]U.C.S.D. Center for Energy Research 9500 Gilman Dr. La Jolla, CA. 92093, USA
[5]Forschungszentrum Jülich, 52425 Jülich, Germany
[6]Sandia Laboratories, P.O. Box 969 / MS 9161, Livermore, CA, 94550-9610, USA
[7]ITER ORG. Fusion Science and Technology Dept., Cadarache - Building 523
13108 St. Paul-lez-Durance, France
[8]Sandia Laboratories, Org. 1111, MS 1056 Albuquerque NM 87185, USA
[9]FOM-Rijnhuizen, Postbus 1207, NL-3430 BE, Nieuwegein, The Netherlands

This report was prepared as an account of work done by a subcommittee of the ITPA (International Tokamak Physics Activity) SOL/divertor group. The opinions herein represent those of only the authors listed and not of the SOL/divertor group in general nor the ITER or IEA organizations (this work started when ITPA was legally under IEA and has continued while ITPA is currently operated under the aegis of the ITER legal framework).

The projections to ITER given in this report are a 'most probable' outcome based on our pooled knowledge and compromises on a range of opinions. If one took into account the full range of possibilities for all physics and materials range of projections to retention in ITER would be so large as to be useless. Thus any range in the projection for a given material or situation does not necessarily represent the underlying uncertainty (or error bars) but a range of conditions that we deem 'probable' at this point in time.

Abstract:
While one goal of this study was clearly to construct projections to T retention in ITER operation a requirement for this work was that it be as transparent as possible, thus allowing interested readers to understand the foundations (in some cases quite weak) of those projections. This study examined the assumptions underlying tritium retention in materials and, based on assessments of applicable data ranges for each parameter, made projections to ITER. Those projections were done for two limiting cases of main chamber fluxes, low (10^{23}/s), and high (10^{24}/s), as well as for the standard ITER materials of Be first-wall, CFC strike points, W baffle and dome as well as 3 other cases: all-C, all-W divertor and Be first wall, and all-W PFCs. In general a fully-C first wall would be most probable to lead to the highest T retention due to carbon's characteristic longer distance movement to shadowed areas (compared to Be) and higher T/C for a given surface temperature. While the standard Be/C/W materials selection was found to probably lead to lower retention rates than for all-C PFCs, replacing the CFC strike point region with W appears to lead to a small (far within uncertainties) reduction in co-deposition due to the relative importance of the main chamber Be source. The retention in the W sections of the divertor due to implantation will likely be small compared to that of co-deposition of T with Be or C in all cases. The T retention projections of this study do show that it is probable that an all W ITER would have the lowest T retention levels. The uncertainties associated with the predictions of T co-deposition with C

or Be lay primarily in the transport physics in the plasma after the Be or C are eroded. In contrast the uncertainties in T retention in W are mostly in the specification of ion fluxes to the surfaces and the physics of traps and T transport in the bulk. Retention of T in the bulk presents a different challenge to T removal than co-deposition on the surface. In all cases higher surface temperatures should reduce retention.

1. Background on the formation of this panel

As will be discussed later in this report there have been a number of studies aimed at predicting T retention in ITER based on current knowledge and comparing the effect of various PFC materials. Such studies have generally been the work of a few individuals and/or the general emphasis of one national group (e.g. the EU). Most recently efforts in both the US and EU occurred as part of the review of the ITER physics and engineering design (summer, fall of 2007). In reviewing that work at the ITPA SOL/divertor meetings it became clear that there were many differences in assumptions and techniques between the EU and US studies. It was felt that by bringing those two groups together and providing much more detail about assumptions and techniques we could potentially provide the general community and ITER with a broader input and consensus. So this effort aimed to gather a broader database of relevant information, evaluate its relevance, and use it to project to ITER. In addition, the meeting was useful from the viewpoint of identifying areas in need of long-term future research, and areas where short-term investigations could provide much needed information almost immediately.

The group organized and met at M.I.T. June 23-24, 2008. This report attempts to document the work presented at that meeting and which occurred over the following 6 months. We hope it can be read by individuals in the field including ITER staff, and utilized as a reference source as opposed to a real prediction of what will happen in ITER. Certainly there are large uncertainties remaining in a number of areas that we hope will be addressed in the future. In addition, any decisions made on PFC materials usage should include not only the issue of T retention but also a number of other, perhaps more important operational characteristics (e.g. dust, PFC lifetime, cost, effects on the core plasma, risks for operation….), as well as what is required for T removal and recovery.

The structure of this report is the following: Following a brief review of past work in this area (section 2) we proceed to review in Section 3 the literature of relevant data and derive either our consensus fit to that data (e.g. retention in W) or make some reasoning to set the limits of required input for calculations (e.g. conversion of eroded main chamber fluxes to co-deposition). Based on the information from Section 3 we divided the main chamber and divertor areas into regions of roughly consistent temperature and fluxes. Section 5 delineates those fluxes and temperatures followed by the projections to ITER of probable retention for a number of different material and flux cases (Section 6).

For future reference the names of individuals principally associated with the work described in each section are listed in the section titles in parentheses. Note that each section will contain a ‘concerns’ paragraph aimed at emphasizing where work is needed (and thus where our assumptions and projections are most uncertain).

2. Introduction (Roth)

The choice of plasma facing component (PFC) materials for ITER is strongly dependent on predictions of heat/particle fluxes as well as the role of the material in tritium (T) inventory build-up in the vessel, which must be limited for safety reasons. The in-vessel tritium limit

has been defined recently to be 700g tritium[1]. The restriction of the use of carbon fibre composites (CFC) to the divertor strike points results both from the attempt to minimize the T inventory and to optimize the lifetime of the PFCs. The selection of Be for the first-wall was based on the belief that the plasma interaction with the main wall was minimal and, if Be entered the plasma, its effect would be minimal. Tungsten was chosen for areas of the divertor to minimize the amount of carbon in the machine and because the erosion lifetime of beryllium components in these regions would be unacceptably short.

A simple scaling of the tritium inventory to ITER, based on a long term retention fraction of 10% of the injected fuel, as obtained in many today's devices, leads to a very limited number of discharges (~ 100) before reaching the safety limit (assuming 200 Pam^3s^{-1} of gas injection with a 50-50% mixture of D-T, resulting in 60 g tritium per 400s discharge) [2]. However, these results are based on all-C devices and could overestimate the retention in ITER with only a C divertor assuming a Be first-wall leads to less T co-deposition with Be than the equivalent all-C ITER. Moreover, the physical basis for such an extrapolation is rather weak; considering the processes involved, the retention rate should scale as the recycling flux on PFCs rather than as the injected flux, although these are often correlated.

More detailed attempts have been made to estimate the T inventory build up in ITER utilizing methods with different levels of sophistication [3-5]. In these evaluations the centre of interest was the plasma interaction with CFC divertor targets and the inventory estimate was based on code calculations for divertor erosion and tritium-carbon co-deposition. Input data for wall and divertor fluxes and flux distribution were taken from the B2/EIRENE model of partially detached ITER plasmas [6]. Results were validated to present devices, e.g. to JET detached divertor plasmas [3] resulting in a co-deposition rate for ITER of 7 mgT/s, corresponding to reaching the inventory limit after about 250 discharges. A considerably improved data base for carbon chemical erosion [4] resulted in more than 1200 discharges before reaching 700 g tritium in the divertor.

In a later evaluation [7] the influence of the vessel wall was taken into account using simple assumptions for a uniform fraction of Be impurity ions in the plasma incident on the divertor. With 1% Be in the divertor edge plasma a tritium retention rate of 15.9 mg/s resulted, being dominated by co-deposition with Be, reducing the number of discharges to ~ 100 before reaching the 700 g limit. Discrepancies especially in describing detached plasma conditions were large and made extrapolation to the ITER semi-detached plasma regime subject to considerable uncertainties.

In the most recent by the EU community the results for C and Be were compared with the case of W [8], where ion implantation was assumed as dominant mechanism and the assessment was done on the basis of existing literature data from ion beams and plasma generators. The extrapolation to long exposure times was done using the experimental $fluence^{0.66}$ power dependence. A rough estimate was made for the additional effect of tritium trapping in n-induced defects in the bulk of W tiles. A similar evaluation of the effect of n-irradiation on the tritium retention in W was performed by the US PWI community [9] yielding similar results.

The main conclusions from the EU community modelling studies of the ITER CFC/W/Be PFC option were that a) co-deposition with eroded carbon from the divertor plates will dominate the tritium inventory (1.25–5 mg/s tritium); b) Tritium co-deposition with eroded Be from the vessel wall is more uncertain due to larger uncertainties in the wall fluxes and uncertainties in the Be transport to the wall or divertor, but could contribute significantly to the total inventory (0.25–1.5 mg/s tritium); c) Implantation of T in the W sections of the divertor was found not to be limiting, although n-irradiation after years of D/T will increase

the retention (estimated range: non-linear with fluence, <0.12 mg/s tritium). The effect of n-irradiation is highly uncertain and requires much more experimental and modelling work; d) The EU study of the W divertor/Be first wall option (remove CFC from the strike points), presently foreseen for the activated phase of ITER, reduces the tritium retention, extending the number of discharges until the tritium limit is reached to about 3000.

All the above assessments concentrated on the divertor as dominant source for erosion and co-deposition and put the level of sophistication on the refinement of input data for erosion, sticking coefficients, re-erosion and final co-deposition. In the present assessment an additional route will be evaluated - A direct estimate of the vessel wall erosion and subsequent migration and co-deposition with T at the divertors is made.

3. Assessment of existing data needed for this study

3.1 Main chamber fluxes (Kallenbach, Lipschultz)

Major sources of uncertainty in the estimates of retention are the particle fluxes to the vessel walls. Such fluxes engender erosion (leading to co-deposition if the material is Be or C) as well as directly implanting ions into the material (W). The fluxes also lead to heating of the surfaces which is important in determining the state of the D and T atoms in the PFC material whether implanted or co-deposited. It has been recognized over the past decade or so that there is much stronger cross-field transport in the SOL than thought given that the initial ITER specification was that only charge-exchange neutrals reached those surfaces. The goal of this study was to produce new estimates for time-averaged fluxes to main chamber surfaces in ITER, including ELMs. This information will be used for surface temperature estimates (Section 5 and appendix B) and then T retention estimates (both local and after transport to the divertor).

The details of how SOL profiles are predicted for ITER are given in appendix A.1. The separatrix density and temperature are scaled from a database of existing tokamak data for that region. The resultant empirical prediction is found to be similar to that determined through B2-Eirene modelling. The fluxes to the edge of the grid in the B2-Eirene model lead to wall fluxes of ~ $1x10^{23}$ ions/s. That value is considered to be a lower limit to what will be likely in ITER as there is a large region between the edge of the modelling grid and the first-wall for which, in today's tokamaks, the transport is thought to be convective. To estimate the convective limit to wall fluxes we pursue two methods: The first analysis is based on ASDEX-Upgrade SOL plasmas and interactions with main chamber surfaces for ITER-like conditions. The second analysis utilizes a model of cross-field ion transport driven by convection to predict the convective velocity at the ITER limiter radius. Those disparate empirical methods gave similar values for the radial ion flux density at the limiter radius, ~$1x10^{24}$ ions/s. Given the uncertainties we have agreed to use the range $1x10^{23}$ (based on B2-Eirenne) to $1x10^{24}$ ion/s (based on this empirical scaling) for the various calculations that follow.

The heat fluxes corresponding to a range in affected first-wall surfaces were also estimated in Appendix A. The power reaching the first wall surfaces (limiters and upper divertor) are very uncertain given the difficulty in determining the ELM characteristics at the first-wall consistent with the current ITER assumption of 1MJ, 20-40 Hz ELMs. A second concern is the splitting of ELM (and non-ELM) power between the upper divertor and the main chamber limiters which is not well documented at this time. With those caveats we have estimated the heat reaching all surfaces outside the lower divertor to be in the range up to 22

MW. Based on those heat fluxes we then calculate the surface temperatures at various main chamber locations (Appendix B).

Concerns: More data on SOL profiles at the highest current (and a range in densities) in JET would probably give more confidence in these general wall fluxes. However, the biggest uncertainty probably lies with the fluxes to individual components. We cannot really predict ELM fluxes in general and specifically for the 1 MJ energy limit for ELMs mandated for ITER. Furthermore the 3D nature of the vessel surfaces really requires a 3D calculation to properly understand the variation of particle and heat fluxes, not to mention the local re- and co-deposition of material. The role of neutrals is not well understood as well.

3.2 Erosion rates at first-wall surfaces (Doerner, Roth, Philipps, Whyte)

As discussed in Section 3.1 the eroded first-wall material plays an important role in co-deposition, both locally (e.g. in tile gaps) and remotely at the inner divertor. At the moment our current assessment is that the eroded main chamber Be or C can dominate the inner divertor co-deposition. Given the wall fluxes calculated in the previous section we need estimates of the wall erosion those fluxes engender as well as how much of that eroded material is transported to the inner divertor and co-deposits there vs. locally re-deposited (and potentially co-deposited).

We have assumed a 2% erosion yield for both chemical/physical sputtering erosion of C as well as sputtering erosion of Be at main chamber surfaces. This value is a compromise for several reasons. If one relied on TRIM calculations one would have Be erosion yields of ~ 5-7%. Ion beam experiments do measure yields close to the TRIM calculated values. However, in plasma devices the sputtering yields are consistently lower than the calculated values. For example, in PISCES, the sputtering yields are a factor of ~3-5 less than TRIM would calculate (see [10]). Results from JET also show erosion yields that are ~5x less than TRIM calculations [11] as well as much larger [12]. We note that the single value for erosion rate is not consistent with the range in parameters used in other sections. But that was what was used.

For the low flux regions of the main chamber the yields for erosion of C are similar for chemical (~ 1%) and physical (~ 2%).

Given the above uncertainties we have kept the erosion yield for both C and Be in the main chamber to be 2%. This has the added advantage of allowing for a better comparison of retention (both local and remotely at the inner divertor) attributed to each potential main chamber material. Also, in spite of the different erosion mechanisms, the interactions (ionization rate, penetration depth into the SOL plasma, re-deposition fraction, etc.) of the different eroded materials in the edge plasma are treated identically.

Concerns: As already discussed above there are differences in the datasets in terms of comparison of ion-beam and plasma experiments and tokamaks that can be quite large for Be. *Here, as opposed to other sections, there was one value chosen (2% erosion) for Be as opposed to a range. That unfortunately gives the reader the impression that this value is certain, which is incorrect. The error bars around any Be result should be large (not estimated) as they are in addition to any uncertainties in Be migration and co-deposition physics. For carbon erosion the same value was chosen; large uncertainties of this value remain in view of the dependence of chemical erosion on the local erosion conditions.* All of those uncertainties could, and should, be reduced. Furthermore, the local erosion rates at the first wall in existing carbon PFC tokamaks (and for Be in JET) are strongly needed to verify whether in fact the predictions of main chamber erosion based on laboratory data are valid for

tokamaks. Such information is also needed in conjunction with the uncertainties in the following section having to do with the level of local re- and co-deposition of eroded materials and how it transports around the tokamak and into shadowed areas.

3.3 Conversion of eroded main chamber material to co-deposits -> material migration (Kallenbach, Philipps, Whyte)

The method of estimating this quantity was strictly empirical, under the assumption that main chamber erosion is the source of C or Be co-deposition at the inner divertor. It ignores erosion and re-deposition (and retention) at the outer and inner divertor plate. Such processes are included only in the plasma and impurity transport code model of the divertor (see Section 6.1b).

Two cases were chosen to cover the range in main chamber ion fluxes described in section 3.1: Low flux ($1x10^{23}$/s) and high flux ($1x10^{24}$/s). In the low flux case all the eroded material is assumed to be transported to the divertors and leads to co-deposition. In the high flux case we have assumed that 50% of the eroded material is transported to the divertors. **To be frank we have no physics basis for selection of the above fractions of erosion transported to the divertors.** We know that it is not zero as experimental measurements clearly show co-deposition rates at the inner divertor of similar order to that eroded from the main chamber. We feel it is unlikely in the high flux case that all the eroded material makes it all the way around to the inner and outer divertor from main chamber surfaces. That leads to an compromise value of 50% of eroded material being locally re-deposited. Finally, we have not properly dealt with what fraction of locally re-deposited material is co-deposited with D/T atoms (and where).

The net material/impurity eroded from main chamber surfaces is assumed to flow along the scrape-off layer field lines into the divertor, with 80% of the impurity flux being deposited at the inner divertor while 20% is deposited at the outer divertor. This assumption is based on results from surface analysis of deposited layers in JET and ASDEX Upgrade [13-15]. The impurity flux arriving in the divertor is assumed to follow the spatial D-T ion flux density distribution according to B2-Eirene modelling of ITER (case 1084) [6]. We do this for simplicity as we have very little data on this subject. And of course we have not taken into account erosion and redeposition of the material that reaches the inner divertor from the erosion sites in the main chamber nor erosion of divertor material.

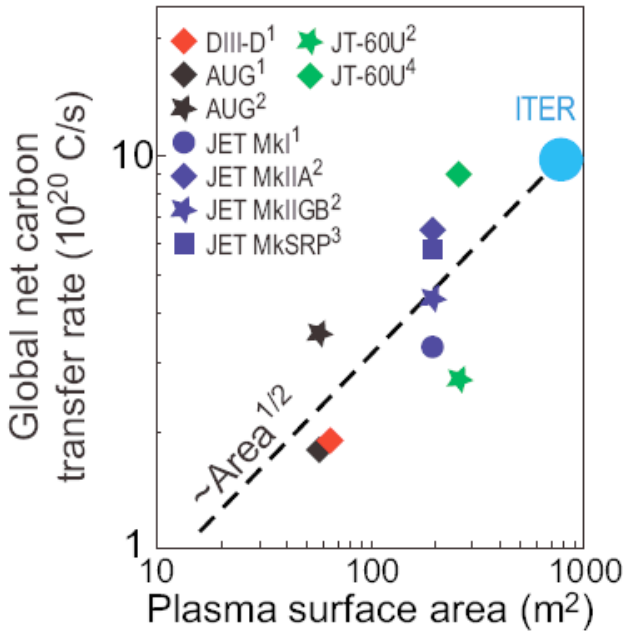

Figure 3.3.1: Data for global transfer rate of C from first wall to inner divertor. Data are taken from a number of references [16-19]

Combining the above assumptions on flow direction and fraction reaching the divertors with that of the previous sections (first-wall particle fluxes and erosion rates) the following material arrival rate at the divertors is predicted and will be used for co-deposition studies:

1. High flux case (2% yield, 50% stays at first-wall, 80% to inner divertor)
flux of Be^+ to inner divertor = .02*0.5*0.8*1x10^{24}/s = 8x10^{21}/s
flux of Be^+ to the outer divertor = .02*0.5*0.2*1x10^{24}/s = 2 x10^{21}/s

2. Low flux case (2% yield, 0% stays at first-wall, 80% to inner divertor)
flux of Be^+ to inner divertor = .02*1.0*0.8*1x10^{23}/s = 1.6 x10^{21}/s
flux of Be^+ to the outer divertor = .02*1.0*0.2*1x10^{23}/s = 4 x10^{20}/s

Note - the above estimates do not include neutral sputtering.

We note that the ERO modelling, shown later, utilizes an assumption of 1% Be in the incoming ion fluxes to the inner divertor plate (0.1% to the outer divertor plate). The ion fluxes to those plates, originating from a B2-Eirene model case, were 2.5x10^{24}/s and 4x10^{24}/s for the inner and outer divertor. The resultant Be+ fluxes assumed are then 2.5x10^{22}/s and 2.5x10^{21}/s respectively. We consider these to be the equivalent of the 'high flux case' from the empirical scaling.

As a separate method of obtaining the rate of first-wall material reaching the inner divertor we reviewed the literature of material accumulation at the inner divertor derived from post-campaign analysis for carbon PFC first-walls [16-19]. The results (Fig. 3.3.1) appear to scale with R or surface area$^{1/2}$. The projection to ITER leads to a value of ~ 1x10^{21}/s although significantly higher and lower values would be consistent with the data. Data from campaign-integrated deposition necessarily integrates over all kinds of plasmas – including Ohmic, low-density, disruptions, ELMs,…. – not constant high-power discharges as assumed for ITER. On that basis the projection of Figure 3.3.1 appears quite consistent with the projection based on the assumptions of the previous sections for the low flux case.

Concerns: The assumptions of this section are in dire need of further support from experimental data. We have made too many assumptions that are ill supported by experimental data or modelling for that matter. Ideally we should have time dependent data for the deposition of C and Be at all main chamber locations and the divertor (+ any sheltered regions in the divertors like a dome) that can be connected back to the corresponding sources at the main chamber and divertor surfaces. In particular we need to obtain a better understanding of what happens to main chamber erosions: What fraction is locally re- and co-deposited? How much transports farther away to surfaces still considered main chamber and at what rate of movement and deposition (and co- vs re-deposition)? What amount is due to neutral sputtering?

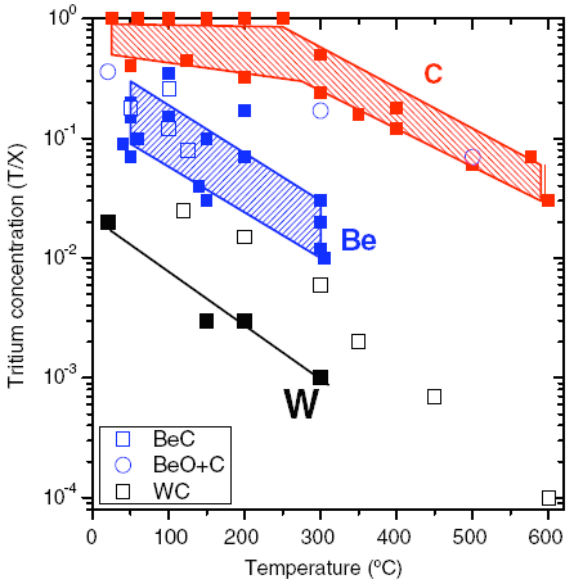

Figure 3.4.1: Data for retention of D co-deposited with C, Be and W.

3.4 Properties of T retained in co-deposited material (Doerner, Roth, Schmid)

The co-deposited tritium retention properties for each of the three first-wall material cases have been assessed. It is well known that the level of hydrogen in co-deposited materials drops with the temperature of the surface during implantation (Figure 3.4.1 [8]). *We note that the effect of raising the temperature **after** co-deposition has not been well studied and should be the subject of future work*. In the case of a tungsten first wall there is very little erosion, and together with low co-deposition fractions (<0.1[20,21]), leads to negligible tritium accumulation due to co-deposits. The situation is much different for co-deposits of T with carbon and beryllium where both the erosion rate and the T concentration in co-deposited surfaces is higher.

The tritium retention properties of the different material co-deposits have been studied [22]. Detailed measurements in PISCES for co-deposition as function of energy, temperature and impurity flux ratio have led to the following equations:

$$(D+T)/C = (2.0 \times 10^{-2}) * E_n^{-0.43} * (\Gamma_{(D+T)}/\Gamma_C)^0 * e^{(2268/T_c)} \quad [T_c \geq 473K]$$
$$(D+T)/C = (2.0 \times 10^{-2}) * E_n^{-0.43} * (\Gamma_{(D+T)}/\Gamma_C)^0 * e^{(2268/473)} \quad [T_c \leq 473K] \qquad (3.4.1)$$
$$(D+T)/Be = (5.82 \times 10^{-5}) * E_n^{1.17} * (\Gamma_{(D+T)}/\Gamma_{Be})^{-0.21} * e^{(2273/T_c)} \qquad (3.4.2)$$
$$(D+T)/W = (5.13 \times 10^{-8}) * E_n^{1.85} * (\Gamma_{(D+T)}/\Gamma_W)^{0.4} * e^{(736/T_c)} \qquad (3.4.3)$$

The equations use the incident particle energy, E_n, the ratio of the two arriving particle fluxes, Γ_D/Γ_X , and the temperature of the co-depositing layer, T_c, to determine the level of tritium retention in the co-deposit. While not used, the retention in tungsten co-deposits is listed for completeness. Details concerning these equations are presented elsewhere [23].

The co-deposited D-T fraction is calculated using the analytical formula (equation 3.4.1-3) with the ion impact energy E and the surface temperature, T_{surf}, and the impurity flux ratio ($\Gamma_{(D+T)}/\Gamma_{Be}$) as input parameters.

The ion impact energy is estimated as $5*T_e$, with T_e taken from the B2-Eirene model for the divertor. Since the ITER divertor parameters (E, T_{surf}) were partly outside the validity range of the analytical co-deposition formula, ($473 < T_{surf} < 973$ K, $15 < E < 100$ eV) its extrapolation had to be specified:

For $T_{surf} < 473$ K in carbon, the value for 473 K was used, in accordance with experimental trends. For $T_{surf} > 973$ K in carbon, the exponential decay of the co-deposited fraction was extrapolated. Regarding the impact of energy dependence, the co-deposited fraction for E=15 eV was used for E<15 eV and the value for E=100 eV was used for E>100 eV.

Concerns: This area appears to be fairly mature and, for the purposes of our work, in pretty good shape. The main concerns are whether the studies that led to the above scaling relations properly cover the right ranges of Be, C and D+T fluxes and their ratios. The question of how varying temperatures after co-deposition affects affects the retained tritium concentrations is presently being addressed and could significantly change the results (e.g. ELMs heating surfaces).

3.5 Implantation of tritium into tungsten (Davis, Doerner, Haasz, Kolasinski, Mayer, Philipps, Roth, Wampler)

In the interest of including a fairly wide range of data we have collected the data from ion beam experiments [24,25], linear plasma generators [26-33] and tokamaks [27,34,35]. We have been more liberal than a previous summary of such data [8] in expanding the energy range to 38-500 eV (staying below the energy of direct trap creation by the implanted ions) and have included

a variety of different W materials. The temperature of W specimens was kept in the range around 500 K. The analysis method for the laboratory data was in all cases thermal desorption spectroscopy (TDS).

The retention data included in this summary are shown in Fig. 3.5.1 as function of incident fluence. In this energy range, the ion-beam studies for fluences of ~10^{21} to ~10^{25} D/m^2 show that the retained amount of D is roughly proportional to the incident fluence to the power of 0.5-0.7 [24,36,25]. Retention measurements in linear plasma devices at higher fluences ($\geq 10^{26}$/m^2) and fluxes (>10^{22}/m^{2}s) evidence no consistent trend among themselves in terms of fluence scaling. For example several studies show essentially no fluence dependence [31,32], while the recent PISCES results at somewhat higher fluence [33] show a fluence dependence comparable to the ion-beam studies.

In order to use the information contained in Figure 3.5.1 in T retention calculations we have fitted limits to the data as shown. As can be seen from the equations included in the figure the upper limit curve follows a fluence$^{0.55}$ scaling. The lower limit curve has a fluence$^{0.66}$ dependence. As is clear from the curves we have assumed that the power law scaling of retention with fluence saturates at the highest fluences. This 'assumption' is not strongly supported in the sense of our real understanding as the results are minimal and mixed with respect to saturation as described above; the TPE and PISCES data have different

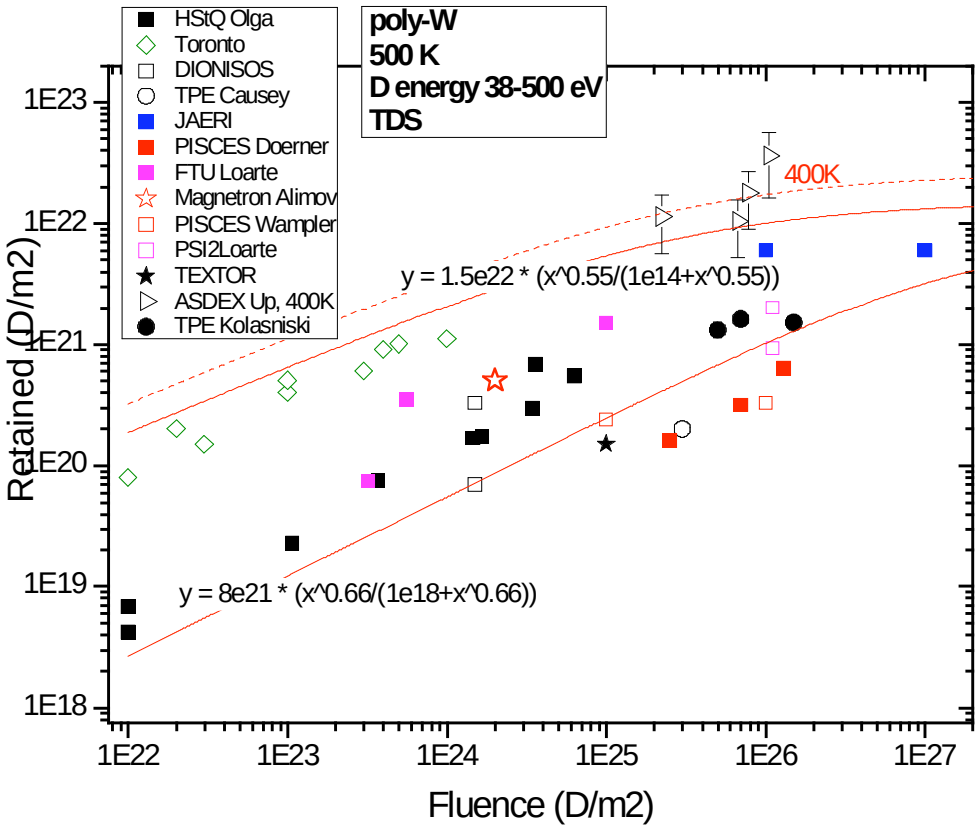

Figure 3.5.1: Data for retention of implanted D in tungsten. Data from the following sources: HstQ Olga [25], Toronto [24], DIONISOS [29], TPE Causey [26], JAERI [31], PISCES/Doerner [30], FTU [27], Magentron/Alimov [28], PISCES/Wampler[33], PSI2 [27], Textor [34], ASDEX-Upgrade [35], TPE/Kolasinski [32].

dependences on fluence. At the same time JAERI laboratory data, at even higher fluences, are

saturated in retention. The JAERI data consists of detailed measurements of the temperature dependence of retention vs fluence while the datapoints in Figure 3.5.1 represent the maximum values. The flattening of the two fitted curves thus comes from a combination of bracketing the experimental data and what we view as the likely probability that the retention will saturate. The saturation level for the fits is given in the figure: $1.5x10^{22}$ and $0.8x10^{21}/m^2$ were assumed. The amount of saturation is clearly debatable.

Figure 3.5.1 also includes data from tokamak experiments for comparison with the laboratory results. Those results are acquired under less controlled conditions, with ranges in surface temperatures and fluxes for each measurement. The FTU and Textor results were acquired with short term limiter tile exposures which, due to the nature of limiter tiles, likely leads to fairly high temperatures, beyond the 500K of the laboratory data in the figure. The ASDEX-Upgrade results were obtained from post-campaign analysis of divertor Langmuir probes manufactured from solid tungsten [15]. As such they experienced the fluxes integrated over a campaign of discharges. Those W samples also experienced the effects of transient temperature increases due to disruptions and ELMs. We note that the ASDEX-Upgrade samples have been assigned an implantation temperature of ~ 400K based on an estimate of average exposure temperatures (averaged over ELMs where there would be very short time period increases in temperature). When that data is scaled to 500K (the temperature of the laboratory data), based on the discussion that follows, the retention drops slightly. Even with all the above caveats the tokamak data falls within the general spread of the laboratory data.

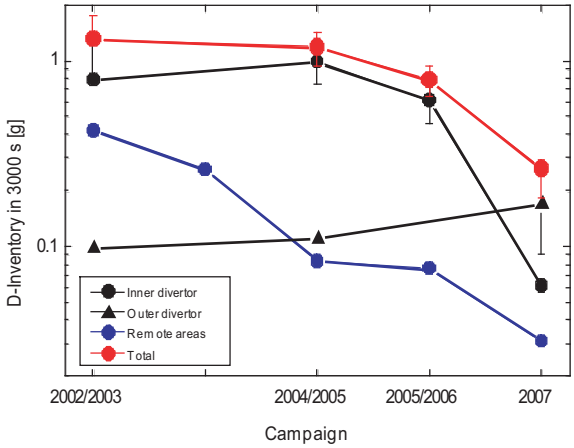

Fig. 3.5.2: D inventory in AUG from post-campaign surface analysis [15].

The ASDEX-Upgrade studies also revealed important information relevant to later discussions comparing retention in carbon vs tungsten. Over a period of 5 years the amount of tungsten-coated surfaces in ASDEX-Upgrade has steadily increased from 0-100%. The campaign-integrated retention for the corresponding campaign periods has been analyzed. The data from that analysis, given in Figure 3.5.2, shows that campaign-averaged retention has steadily dropped as the amount of carbon PFCs is reduced [15,35]. In addition the type of retention has moved from dominated by co-deposition at the inner divertor plates to dominated by implantation at the outer divertor plates (as expected). There also exists ASDEX-Upgrade data for single-discharge retention [37] which indicate a saturation of retention with increasing fluence. Since it is not normalized to the implanting ion flux it cannot be included in Figure 3.5.1.

The other tokamak with all high-Z PFCs is Alcator C-Mod. The material is molybdenum which is comparable in many ways to tungsten in terms of lattice structure and hydrogenic retention. The full campaign-integrated retention [38] is lower than ASDEX-Upgrade, more on the level of the TPE results (~ $2x10^{21}/m^2$ retained for ~ $10^{26}/m^2$ integrated fluence [32]). On the other hand the single-discharge (quiescent, non-disruptive) retention (~ 1-2% retention at an ion fluence of $10^{23}/m^2$) is at or slightly above the upper limit fit in Figure 3.5.1, a factor of 5-10 higher retention than the highest laboratory data at those fluences. The differences between single-discharge and campaign-integrated retention (~ 1000x lower) is thought to be due to disruptions removing retained fuel.

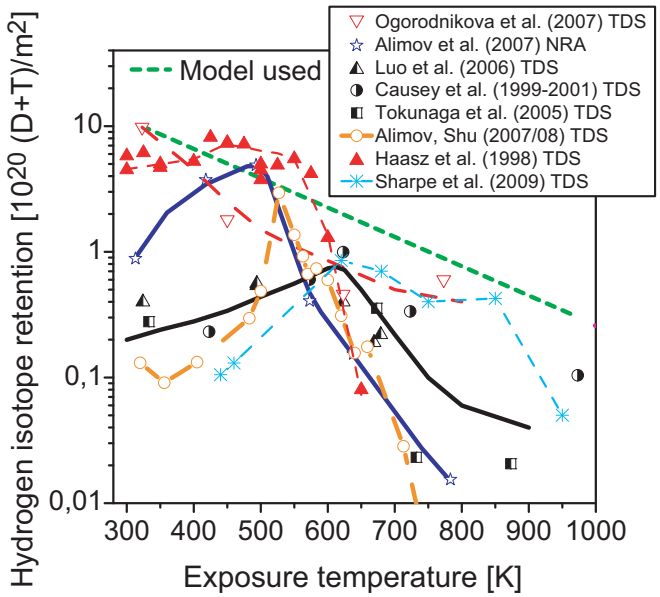

***Figure 3.5.3**: Temperature dependence of the hydrogenic retention in W measured at different ion fluxes and fluences. Ogorodnikova [42], Alimov [41], Luo [40], Causey 1999 [26], Tokunaga [39], Alimov/Shu [31], Haasz [24], Sharpe [32].*

While the data of Figure 3.5.1 only included a limited range of temperatures we must also take into account the temperature dependence which appears to have other dependencies as well. The data of Figure 3.5.3 (some from that of Figure 3.5.1 plus others [24,26,39-42,31,32]) includes a range in temperatures and fluxes as well as fluences (10^{24} – 10^{26} D^+/m^2). To be able to plot all such datasets on the same graph we have scaled the retention to a fixed fluence of $10^{24}/m^2$ under the assumption that retention scales as fluence$^{0.66}$, the lower limit scaling of Figure 3.5.1. We note that above ~500 K, which is most relevant for ITER, the retention generally decreases with increasing temperature. In order to take this effect into account, a common temperature dependence was fitted to the maxima of the temperature dependence of each flux. It is shown in the figure as 'model used' and is given by 57.75xexp(-T/185.), an exponential decay with a characteristic temperature of 185 K.

As obliquely referred to above the data of Fig. 3.5.3 appear to show some flux dependence as well. For the lowest flux [36,25] the retention drops monotonically as a function of temperature. For fluxes above $1x10^{21}/m^2s$ the retention curves exhibit a maximum over a wide temperature range (~400-600 K). The curves which have the highest temperature peaks also correspond to data for the higher fluxes; There may be some decrease in maximum retention with increasing flux as well. The information about where the maximum in retention occurs as a

Author	Implantation	Energy [eV]	Flux [$D/m^2/s$]	Fluence [D/m^2]	technique
Ogorodnikova [42]	D beam	200	$3x10^{19}$	$3x10^{24}$	TDS
Alimov [41]	D plasma	200	$1x10^{21}$	$9x10^{24}$	NRA
Luo [40]	D plasma	98	$1x10^{22}$	$1x10^{25}$	TDS
Causey [26]	D+T plasma	100	$9x10^{21}$	$3x10^{25}$	TDS
Tokunaga [39]	D plasma	100	$1x10^{22}$	$1x10^{25}$	TDS
Alimov,/Shu [31]	D plasma	38	$1x10^{22}$	$1x10^{26}$	TDS
Haasz [24]	D beam	500	$8x10^{19}$	$1x10^{24}$	TDS
Sharpe [32]	D plasma	70	$8x10^{21}$	$1x10^{26}$	TDS

Table 3.5.1: Details of all the data used in deriving the scaling of retention with fluence dependence on material temperature, Figure 3.5.3

function of flux is not included in this study but clearly should be the subject of future work.

Concerns: In general there is considerable laboratory data on hydrogenic retention in tungsten. It is unfortunate that at the highest fluences there is very little data and we are basing our projection of saturation on that. It would be good to have more confidence in that, particularly at the fluxes of ITER which are higher than any of the lab data. At first glance the tokamak data appears to be roughly consistent with the laboratory data shown. More thorough investigations are needed to obtain better statistics (and thus confidence) and to better determine if there are differences between the tokamak and laboratory experience. It will be difficult to construct such experiments under controlled conditions. We are also lacking a reasonable model of implantation and transport in the W that will explain the variations in the data shown and give us guidance as to whether we should expect to observe saturation at the higher fluences or even how the retention should scale with fluence and material temperature.

More specifically the detailed physics of what happens in the implantation region and beyond is the subject of much speculation. For example it has clearly been observed that bubbles are formed, typically a few microns below the surface. Such bubbles appear often to eventually rupture thus limiting the retention and potentially blocking the hydrogen from diffusing further into the material. Better understanding of this phenomena and its dependence on fluxes, grain size and orientation would be helpful for retention as well as for dust formation. Another process that may lead to reduced T retention is the simultaneous bombardment with He. There is also the possibility (based on C-Mod results) that multiply-ionized impurities in the plasma (Be, C, O) are being implanted at high energies into the tungsten and directly creating traps there, a process that would increase retention but unlikely to occur in laboratory plasmas.

4. Neutron damage which leads to enhanced fuel retention in tungsten

4.1 Neutron damage effects (R. Kolasinski, W. Wampler, D. Whyte)

Fusion neutrons produce displacement damage in materials. Tritium atoms injected into tungsten from the plasma diffuse through the metal lattice and may become atomically bound at lattice defects, referred to here as trapping. Vacancies, vacancy clusters and voids are particularly effective traps for hydrogen in metals [43]. Here we consider the potential impact of such trapping on tritium retention at neutron damage sites in tungsten. The amount of damage is characterized by the number of displacements per metal atom (dpa). The damage rate can be calculated from the flux and energy spectrum of neutrons using collision cross sections from nuclear data libraries [44]. Such calculations for ITER are reported in the 2004 ITER Nuclear Analysis Report [45], which gives an end of life damage level of 0.7 dpa for tungsten in the divertor from a neutron power fluence of 0.26 MWa/m^2 at a rate of 0.4 MW/m^2 for 0.63 full power year (FPY) or 2x10^7 full power seconds (FPS). The corresponding damage rate is therefore 1.1 dpa/FPY or 0.35x10^{-7} dpa/FPS, or 2.7 dpa/MWa/m^2. Converting the neutron power flux to the equivalent particle flux ϕ_n of 14 MeV neutrons, this damage rate can be expressed as a cross section for damage production of s_d = 2.0x10^{-21}cm^2 [46], where the damage rate is given by $s_d \phi_n$.

The number of defects and trap sites for tritium is less than the number of dpa because many of the defects anneal. For example, in tungsten, interstitials are mobile and recombine with vacancies below room temperature. Vacancies are mobile and anneal at temperatures above about 600K [47], whereas vacancy clusters and voids are stable to higher temperatures. Experiments are therefore necessary to establish the concentration of hydrogen isotopes retained for a given displacement damage.

Figure 4.1.1 shows a summary of several studies of the increase in deuterium retention due to

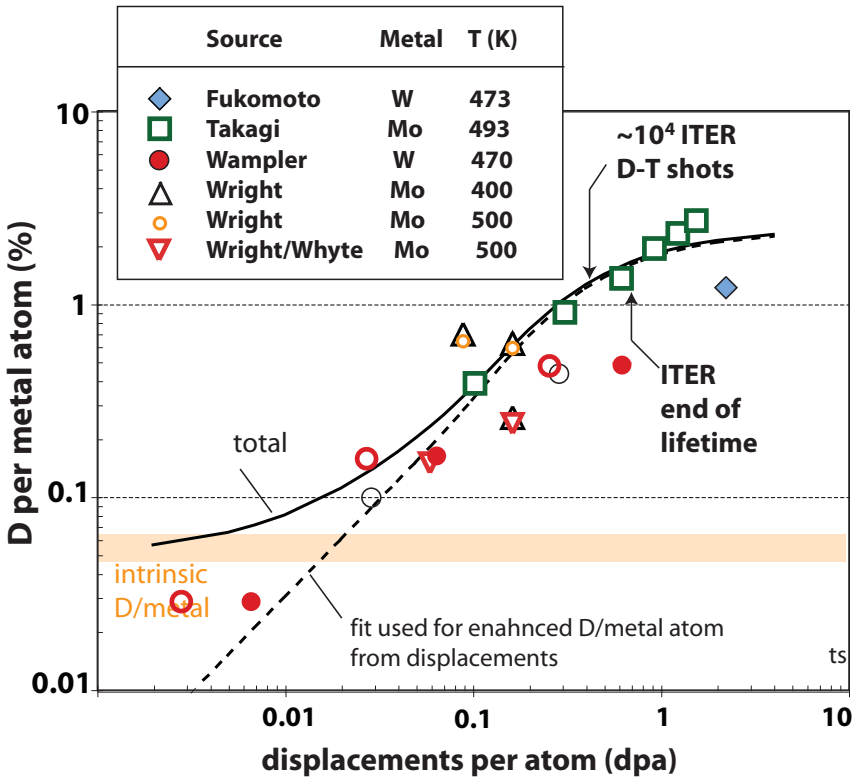

Figure 4.1.1. The **increase** in deuterium concentration due to damage from ion irradiation in tungsten [48-49] and molybdenum [29, 50-51].

displacement damage in tungsten [48,49] and molybdenum [50,29,51] near 500K. Molybdenum was included because of the dearth of related data and because in general hydrogenic retention in Mo is similar to that in W. Note that an assumed level of intrinsic traps in W of ~ $5x10^{-4}$ [24] was used and is shown as a horizontal band for reference. This is a conservative assumption as other studies have found lower levels, the value of which depends on processing. In these studies, damage was produced by energetic ions rather than neutrons. This produces damage similar to that of neutrons, but localized near the surface and peaked near the end of range of the ions which is typically a few microns. The damaged metal samples were subsequently exposed to a high fluence of low energy deuterium from a plasma to simulate ITER plasma exposures. The resulting deuterium concentrations were then measured versus depth, in most cases by nuclear reaction analysis, which typically has a maximum depth of analysis of a few microns. Figure 4.1.1 shows the **increase** in D concentration due to the damage, averaged over the damage profile, versus dpa. The dpa is calculated based on an average damage over the range of the damaging ion using SRIM (not just at the peak damage location) [52]. In these calculations a value of 40 eV for the displacement threshold energy was used for consistency with the damage calculations reported in the 2004 ITER Nuclear Analysis Report [45]. This displacement threshold energy is consistent with values from electron irradiation studies, although higher values are reported for damage from ion and neutron irradiation [53]. Figure 4.1.1 thus provides the relation between damage and maximum concentration of D (or T) that is trapped at this damage assuming that the T, implanted at the surface, can reach that location.

As shown in figure 4.1.1, the concentration of trapped deuterium is about 0.01 D/W for the 0.7 dpa end of life damage in ITER. Assuming 50%D and 50%T, this corresponds to an increase in tritium inventory with damage at a rate of $7.1x10^{-3}$ T/W/dpa or 2.2kg/(m^3 dpa) or $7.8x10^{-5}$ gram/(m^3 FPS) in ITER. The impact of this on tritium inventory in ITER depends on the volume of tungsten throughout which this trapping extends. Since the damage from neutrons extends throughout the entire volume of tungsten in ITER, there is the potential for tritium to be trapped at this damage throughout the entire volume. This would give a large contribution to the tritium inventory of 0.16 milligram/FPS in the divertor (210m^2 x 0.01 m thick tungsten) and 0.53 milligram/FPS in a tungsten main chamber wall (680m^2 x 0.01m thick), reaching an end of life inventory of 3.3 kg in the divertor and 10.7 kg in the main chamber wall assuming it is tungsten. However, it is presently not known whether tritium retention at damage will extend to depths of a centimeter. No data is available that give D retention at displacement damage in tungsten from exposure to plasma at depths greater than a few microns. Haasz et. al. reported D concentrations of ~ 0.001 D/W extending to 25 microns in undamaged tungsten foil after implantation with 500 eV D at 500K [24], but these were intrinsic traps of unknown type not produced by displacement damage. Furthermore, the rate of tritium uptake may be limited by the rate at which tritium can reach the traps rather than by the rate of trap production, particularly on the vessel wall where lower fluxes lead to slower uptake.

For the purposes of modelling we need to abstract from Figure 4.1.1 a general algorithm for describing the D/W as a function of dpa: The fit, shown in the figure, is:

"displacement damage": D/atom = 0.03*dpa + exp(-0.4/dpa)*(1.2e-2 - 0.03*dpa) (4.1.1)

"total": D/atom = 5e-4 + 0.03*dpa + exp(-0.4/dpa)*(1.2e-2 - 0.03*dpa) (4.1.2)

Given that formulation and the rate of damage in ITER we can also predict the rate of trap site creation for an all-W ITER as shown in Figure 4.1.2. Note that although the ion fluence to main wall surfaces is lower than for the divertor the potential for trapping is higher there due to its larger area.

Tritium uptake can be modeled by numerical simulations, which include diffusion, trapping and detrapping. These can also include spatial and temporal variations in temperature and incident flux of DT onto the surface from the plasma. However, such simulations may not include important physical mechanisms such as precipitation as gas into internal voids, and thermal annealing of defects, which may strongly influence tritium retention. The presence of blisters on the surface of plasma-exposed tungsten (e.g. [54]) is evidence of gas precipitation. At the higher temperature, D retention may be reduced by annealing of the damage. Thermal annealing of vacancies is expected to reduce the concentration of traps and in tungsten occurring at 773K but not at 473K. The current situation is therefore that there is a possibility of a large contribution to tritium inventory from trapping at neutron damage in tungsten to large depths, but also a large uncertainty whether this will actually occur since it has not been experimentally verified. Experiments to resolve this uncertainty should be a high priority.

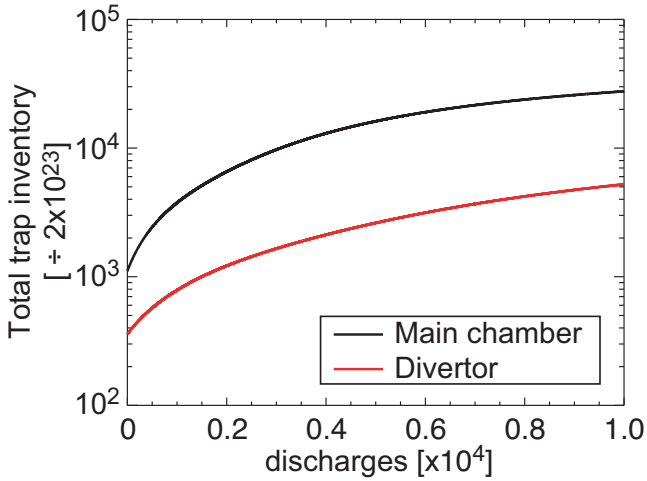

***Figure 4.1.2**: Prediction of the amount of traps in ITER, due to neutron damage, vs shot. Note that this is only for full Q=10 400s discharges.*

Concerns: Clearly the understanding of conversion of dpa to traps and the characteristics of those traps are at an early stage. More information is needed on the trap formation and its dependence on a number of factors from temperature to whether the simultaneous ion irradiation has an effect on the conversion efficiency (e.g. by filling traps before they are lost). Another issue is will the T get to the traps? Will surface bubbles effectively block diffusion into the bulk?

4.2 Analytic formulation for trapping of T in W (W. Wampler, D. Whyte, R. Kolasinski, B. Lipschultz)

As a check for the models described later we first look at a simple analytic formulation for the amount of T diffusing in and being trapped at sites in the bulk. This is an overestimate because one assumes a constant trap fraction (1% concentration) for all operation as opposed to the time dependence as shown in Figure 4.1.2. Furthermore the effect of detrapping is not taken into account. The parameters used in analytic formulation are defined below:

$\Phi =$	incident flux
$r =$	implantation depth
$D =$	Diffusivity
$R =$	Recombination rate
$t =$	irradiation time
$C_{Sr} =$	concentration of mobile H in solution at the implantation depth
$C_T =$	trap concentration
$C_{Ss} =$	surface concentration of H in solution sites
$x =$	depth to which traps are filled as a function of time
$I =$	Inventory as a function of time
$A=$	PFC area
$K_R=$	Surface recombination rate for hydrogen

Based on the analytic formulation [55] the following relationships were used for the diffusion only case:

$$C_{Sr} = \Phi r / D$$
$$x = \sqrt{\frac{2DtC_{Sr}}{C_T}} \qquad (4.2.1)$$
$$I = xC_T = \sqrt{2DtC_{Sr}C_T}$$

When one includes recombination at the surface the flux back to the surface from the implantation depth, r, depends on the concentration gradient, i.e. on the surface concentration of hydrogen. The equations change slightly: The surface concentration, C_{Ss}, is determined by the recombination rate according to $\phi_D = K_R C_{Ss}^2$ (The molecular flux, $\phi_{D2} = 0.5 \bullet K_R C_{Ss}^2$). At the same time $\phi_D = D(C_{Sr}-C_{Ss})/r$ because the flux back to the surface is in series with the flux out of the surface (and ~ equal to the flux of ions being implanted).

$$C_{Ss} = \sqrt{\Phi / R}$$
$$C_{Sr} = C_{Ss} + \Phi r / D \qquad (4.2.2)$$

I and x can then calculated as shown earlier.

In a review of the literature it is clear that there are divergent opinions on the subject of surface recombination rate. A sampling of studies and the recombination rates has been included in this work and is shown in Figure 4.2.1. They include:

(a) Infinite: C=0 at the surface
(b) Pick model [56]: $K_r = 3.0\text{x}10^{-25}/T^{0.5}$ exp(2.06 eV/kT)
(c) Anderl [57]: $K_r = 3.2\text{x}10^{-15}$ exp(-1.16 eV/kT)

(d) Wright [29,51], using Mo as opposed to W: $K_r = 2.0\text{x}10^{-28}$ exp(-0.25 eV/kT)

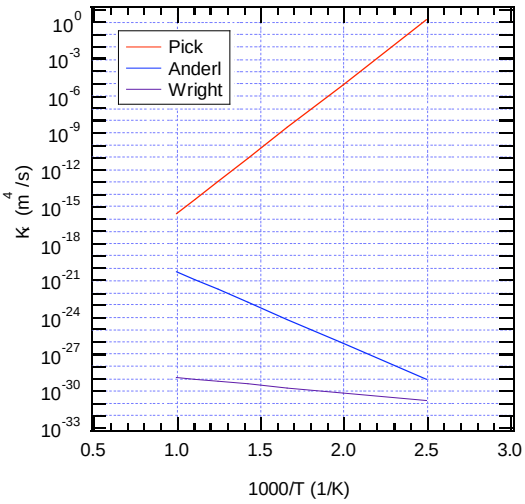

Figure 4.2.1: Surface recombination rates as a function of 1/temperature.

We note that amongst the authors of this study the majority subscribe to the opinion that properly cleaned high-Z surfaces should have very high recombination rates, most likely of the level predicted by the Pick model. Impurities on the surfaces will lead to reduction of the recombination rate (e.g. [58]). However, the uncertainties expressed by some of our group, together with the concern not to ignore a potential enhancement of retention, has led us to include in this study the effect of the range of recombination rates determined by the experimental results of Anderl [57]and Wright [29,51]. We note that strictly speaking the Wright data are for Mo (another refractory metal), but are in good agreement with other experiments on W that also found similarly low recombination coefficients [59,50]. A further complication to the surface model is that tritium can precipitate into near-surface cavities or bubbles which will reduce the near-surface solute concentration and reduce the rate at which deeper traps are filled. Also it is likely that higher temperature operations could anneal some damage, although the efficiency of this annealing is unknown for the range of expected ITER W temperatures.

Concerns: It is generally agreed by the authors that the surface model is critical to predicting the possible T retention rates in W, i.e. the surface concentration will set the rate at which volumetric traps, both intrinsic and neutron-produced, can fill up. However there is not agreement as to the most likely surface conditions that will be present in ITER. This is a reflection of the extremely large scatter in the experimental/theoretical results themselves; e.g. the many orders of magnitude difference in recombination coefficients. In some cases, such as precipitation into bubbles, we presently do not have a quantitative model, and the experimental results for precipitation are also mixed. Therefore, while this is likely important we are uncertain as to how to implement these effects in the numerical modeling (of course the presence of such bubbles may impede tritium retention but may simultaneously degrade the surface properties of the W). So while we identify this subject as a critical research item, for the purposes of this report we have moved forward by using the two extremes for the assumption of surface recombination: namely 1) an "optimistic" case where the recombination rate is taken as infinite and therefore the surface concentration is the *minimum* it can be based on simple ion implantation and diffusion and 2) the "pessimistic" case of the lowest recombination rates taken from Wright et al. (which are actually derived from measured solute D concentrations during plasma exposure). This helps to both frame the possible ranges of T retention, and to understand the sensitivity of the global T retention rate to the surface model assumptions, which is not easily seen unless one works through the effects at all the different W wall section of ITER with their different ion flux, temperature, etc. conditions. In fact, this scoping study shows that despite the enormously different assumptions in surface recombination the resulting enhancement is at most a factor of ~10 comparing the optimistic (10,000 shots to retention limit) to pessimistic case (~1000 shots to retention limit). Obviously, this difference falls into the range where it may matter to ITER

operations. On another positive note we are beginning to get data at very high fluences, $10^{27}/m^2$ [31], a level approaching 2500 discharges for the ITER divertor.

4.3 Modelling of permeation and trapping of the T in the W lattice (R. Kolasinski, D. Whyte)

Appendix C includes a general comparison of available codes that occurred before the MIT meeting in June of 2008. The goal of that exercise was to determine if the basic numerics of the various codes agreed and whether there were advantages of one code over another. Based on those results and the availability of people to run them 2 were selected for this study, TMAP [60] and WW [61].

Both TMAP and WW models can account for the gradient in temperature between the front surface and the coolant channel, held at 425K. TMAP assumes an implantation profile in the material that is Gaussian in space with width 1nm. WW places the implantation source at one grid element. Both codes have assumed, for this exercise, that the implantation depth in nm is 0.1x the implantation energy in eV. While WW can account for the changing trap densities vs. time (Fig. 4.1.2) TMAP cannot and assumes a constant total trap density of 1% corresponding to the full ITER lifetime.

A listing of relevant input parameters is given below:

Trap energy (defined here as the energy of D in a trap relative to solution, 1.06 eV, plus the activation energy for diffusion, 0.39 eV): 1.45 (eV)
Trap density: 10^{-2} (/W)
Diffusivity (H): $D=4.1\text{x}10^{-7}*\exp(-0.39/8.625\times10^{-5}/T)$ (m^2/s)
Solubility: $S=1.83\text{x}10^{24}\text{x}\exp(-1.04/8.625\text{x}10^{-5}/T)$ ($1/m^3Pa^{1/2}$)
Maximum computation time step: 1 sec (TMAP)
Trap rate: $D/(3.147\text{x}10^{-10})^2$ (s^{-1})
Release rate: $10^{13}*\exp(-1.45/8.625\text{x}10^{-5}/T)$ (s^{-1})
Note: For the calculations described here the diffusivity listed above was corrected for tritium.
PFC thickness: 10 mm

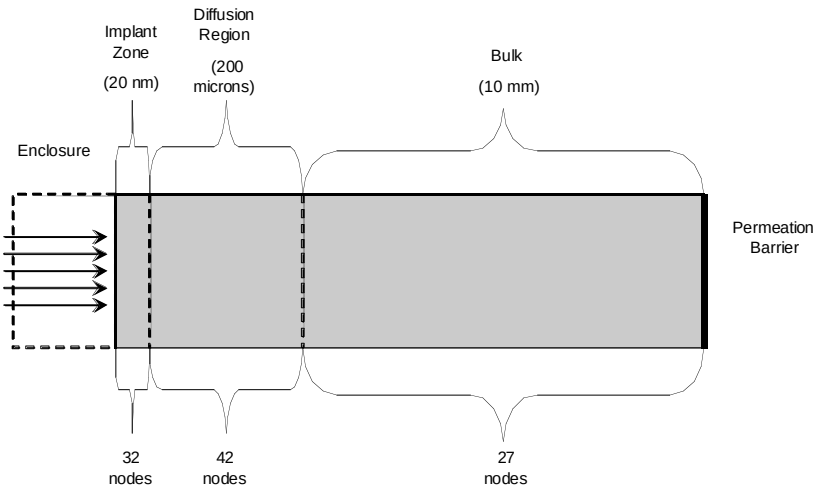

Figure 4.3.1: TMAP simulation layout.

All implanted flux is assumed to be tritium such that the Frauenfelder diffusivity is assumed for T. After the calculation is done then only half the trapped T is really T, the other half D. To simplify the calculation further we have combined the neutral and ion fluxes detailed in the table of Appendix B. That means we use a total incident flux (the sum of the ion and neutral fluxes). The energy ascribed to that total incident flux is the flux-weighted average of the 2 species.

Once the details of the actual ITER regions was specified it was clear that a wide range of conditions would need to be properly modeled by these codes. And so a second comparison study was launched in order to make sure such issues as the surface models and detrapping were being handles properly. Appendix C includes a direct comparison of the TMAP and WW codes for three different flux regions in ITER ranging from high to low flux for the case of infinite recombination at the front surface. The comparison was helpful in tuning the codes to properly model the situation over different time and spatial scales.

Concerns: These models are simple models of hydrogenic diffusion through the tungsten containing atomic trap sites. They are not meant to encompass the details of what happens during the ion implantation and near surface dynamics discussed in Section 3.5 and the same issues arise here. Better models for the retention resulting from ion implantation (and the resultant damage to the material) will also make the models of what happens overall including neutron damage better. Further studies of the transport and retention of hydrogen in tungsten, and the influence of damage and precipitation, are needed.

5. Surface temperatures (B. Lipschultz)

The surface (and bulk) temperature of the location where T is retained is as central to the calculation of T retention as the material properties, reviewed in the previous section. To this end we have utilised the wall fluxes of Section 3.1 to obtain the local fluxes and temperatures of main chamber surfaces. The details and summary of those calculations are given in Appendix B. T_{surf} is calculated assuming 2 different thermal conductivities for the divertor CFC: κ=50 W/(mK) for irradiated CFC and κ =150 W/(mK) for non-irradiated CFC. The former is for neutron-damaged NB31. The latter conductivity is for the average conductivity (pan/pitch) for NB31 and also applies to W. The through-thickness distance to the coolant channel (held at 125°C) was assumed to be 1 cm in all cases in calculating the equilibrium surface temperature.

The fluxes to divertor surfaces are relatively straightforward. We utilized a calculation by Andre Kukushkin using B2-EIRENNE for the particle and heat fluxes (see Appendix A). Because the official divertor surface area is 220 m^2 and the B2 EIRENNE regions with non-negligible amounts of ion and neutral flux total 112 m^2 we have adjusted the main chamber area to include extra area beyond that officially ascribed to it (680 m^2); 108 m^2 of low ion and atom flux, corresponding to the missing divertor area (the upper regions of both divertor areas) was added to the main chamber surface area for a total of 788 m^2.

The fluxes to the 788 m^2 of main chamber surfaces (derived in section 3.1) have been further broken up into 5 regions (see Appendix B). These include the upper divertor (35 m^2), the high flux regions of limiters (50 m^2), both of which experience ELM heat loads. In addition there are fluxes to the wall between limiters (315 m^2, including the tops of the inner and outer divertors) as well as shadowed regions between limiters (215 m^2) and regions of the wall that only experience atom fluxes (177 m^2). The areas and corresponding fluxes given are estimates assuming the walls are covered with limiter surfaces that vary in radius as one

moves toroidally; at each point poloidally the flux to the surface varies toroidally in a repetitive peak and valley.

All of the above information as well as the specifications for surface temperatures, ion and atom flux as well as energies can be found in Appendix B.

Concerns: Of course the surface temperature calculations are only as good as the description of the plasma fluxes and plasma characteristics of Section 3.1 and Appendix B. Furthermore ITER is considering a variety of cooling channel temperatures which will correspondingly vary the front surface temperatures.

6. Projections to ITER

The review of the existing database of information and statement of assumptions in the previous sections serves as the foundation for making projections of T retention to ITER. What follows in this section should not be perceived as a prediction of ITER inasmuch as we have, as yet, been unable to really put uncertainties on the data and assumptions of the previous sections. The reader should view the projected retention in ITER as a guide based on our current knowledge that this group has agreed upon. If asked a year from now to revise this projection it could likely be very different.

In making the calculations that follow we have pursued two methods -

Method 1 – strictly empirical, scaling from the data of section 3.

Method 2 – Primarily using codes (ERO & DIVIMP) but with some ad hoc assumptions based on experiment.

Using the above methods we have addressed four combinations of surface materials and techniques used to project to ITER:

1a) Be main chamber, C/W or all W divertor (method 1 & 2)

1b) Be main chamber, C/W divertor (method 2)

2) All – carbon PFCs (method 1)

3) All – tungsten PFCs (method 1 with, and without neutron damage effects)

6.1a Empirical projection of T retention in ITER assuming that all retention is due to T-Be co-deposition in the divertor (the source of Be being main chamber walls), (A. Kallenbach)

The method of estimating this quantity was strictly empirical, under the assumption that main chamber erosion is the source of Be co-deposition at the inner (80%) and outer (20%) divertor. It ignores erosion of the C divertor (and thus co-deposition due to C). Erosion of main chamber PFCs by neutrals is not included. The local to the main chamber re-deposition and co-deposition of Be with T is not included either. The implantation into the full W divertor is ignored but can be obtained by looking at the second material combination – 6.2.

The assumptions of the material flow to the divertor together with surface temperatures and the corresponding co-deposition values are used to calculate the co-deposition rate at each divertor grid element. Then we integrate over the divertor to obtain the following:

κ = 150 W/(mK)

Case	Inner div. retention	Outer div. retention	Total in 10^5s

Low wall flux	1.80×10^{19} T/s (0.09 mg/s)	5.25×10^{18} T/s (0.03 mg/s)	12g T
High wall flux	1.26×10^{20} T/s (0.63 mg/s)	3.7×10^{19} T/s (0.18 mg/s)	82g T

κ = 50 W/(mK), hotter targets:

Case	Inner div. retention	Outer div. retention	Total in 10^5s
Low wall flux	6.25×10^{18} T/s (0.03 mg/s)	1.95×10^{18} T/s (0.01 mg/s)	4.1g T
High wall flux	4.38×10^{19} T/s (0.22 mg/s)	1.37×10^{19} T/s (0.07 mg/s)	29g T

Table 6.1.1: Empirical estimates for the tritium retention rates for ITER divertor plates. Co-deposition with wall-source impurities is assumed as dominant mechanism. Calculations are done for Be walls and thus Be co-deposition. Two different heat conductivities of the CFC target material are assumed.

Concerns: As expressed above we have not dealt with the erosion of the local material (carbon) in the divertor and the resultant co-deposition with D and T. We have also not dealt with the migration of C or Be to shadowed regions both in the divertors as well as along the way from the main chamber to the divertors. The latter poor state of affairs, including the lack of a realistic range for Be erosion rates, was already brought up in section 3.3. Lastly there is likely migration from the outer divertor to the inner divertor, which is not taken into account. There has been some discussion that JET and ASDEX-Upgrade data might give us some idea of what the level of that material transfer is. In general, in both these empirical calculations as well as the ERO and DIVIMP models to follow, the effect of transient heating (ELMs, disruptions, H-L transitions…) will lead to erosion of poorly adhered (and poor thermal contact) deposition layers. Such an effect is not taken into account.

6.1b Model projection of T retention in ITER with Be walls (Standard C/W divertor (A. Kirschner, K. Schmid)

Two models were used to calculate the T retention in ITER. The first calculation uses the DIVIMP code and assumes an all-W divertor and Be walls. Erosion at main chamber surfaces is directly calculated as well as the transport of that material to the inner and outer divertors. The second calculation utilizes the ERO code with the current ITER selection of materials (Be/C/W). In contrast to the DIVIMP code the main chamber Be source is directly assumed. That source is treated as an influx into the two divertor regions.

The first modelling effort, using DIVIMP, determines the Be erosion by extrapolating the ion fluxes and plasma temperatures from the boundary of the DIVIMP calculation grid towards the ITER first wall. The details of that calculation can be found in [62]**.** At the Be main chamber wall the D ion fluxes are in the range from 10^{19} to 10^{20} (m^{-2} s^{-1}) and the D ion energies are of the order of a few hundred eV. Be Erosion at the first wall is dominated by D and Ar ions. Note that the lower limit of the ion fluxes used for empirical scaling of Be erosion, averaged over 680 m^2, was $1.5x10^{20}/m^2/s$. The poloidal distribution of D-CX flux is similar to that of the D ions. The highest fluxes occur in the divertor with energies below 10eV. The highest average D-CX energies are found in the main chamber but the CX-flux is much lower.

The average Be erosion flux is $6x10^{18}$ (m^{-2} s^{-1}) which corresponds to ~0.05 nm/s. It shows a pronounced minimum at the location of the upper divertor due to the low plasma temperatures at this location. The total amount of eroded Be at the main wall when integrated over the entire surface area of the first wall amounts to $2x10^{21}$ Be/s., again, similar to the levels obtained in the empirical evaluation of Be erosion (section 3.3) for the low-flux case.

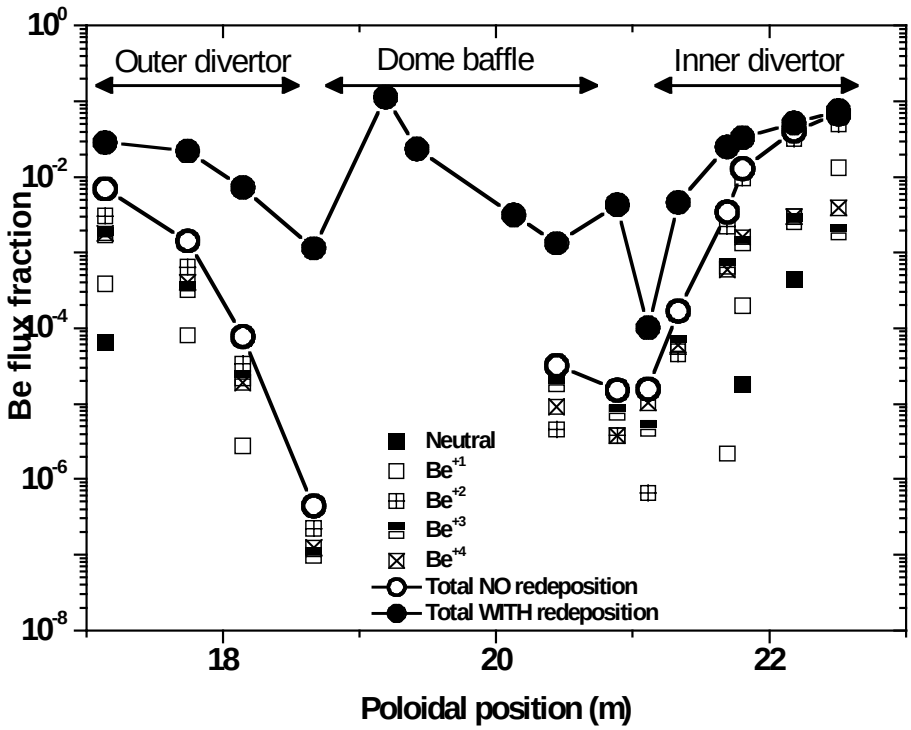

Fig. 6.1.1: Be flux fraction (Γ_{Be}/Γ_{D+T}) arriving at the ITER divertor. Square symbols show the charge resolved Be flux distribution due to main wall erosion alone. Filled circles show the charge integrated Be flux distribution including the effect of re-erosion and re-deposition. This figure is taken from [62] (figure 11).

The initial Be flux into the divertor is ~20% of the Be eroded in the main chamber. The rest of the main chamber Be source is initially re-deposited in the main chamber. This does not mean that it stays there because it is re-eroded and makes a step-wise transition into the divertor since the main wall is Be erosion dominated.

The fraction of Be in the particle flux onto the divertor surface ('Be flux fraction') calculated with DIVIMP due to main chamber Be erosion as the only source is shown as open symbols in Fig. 6.1.1. The open circles show a strong inner outer divertor asymmetry. The flux fractions at the inner divertor are higher than in the outer divertor. The maximum Be flux fraction of 0.06 is found at the baffle at the inner divertor entrance. The maximum Be flux fraction in the outer divertor is roughly an order of magnitude lower as was assumed for the empirical calculations of section 3.3. No Be flux at all is found on the outer part of the dome baffle. The influence of re-erosion and re-deposition after the initial Be deposition step has a strong influence both on the Be flux fraction distribution and on the Be layer growth in the divertor . The closed symbols in Fig. 6.1.1 show the Be flux distribution including the effect of re-erosion and re-deposition. These two processes make the Be flux fraction distribution poloidally more homogenous and strongly increase it to percent levels on average.

With respect to Be layer growth the outer divertor is still erosion dominated and the inner divertor deposition dominated. The main difference when including re-erosion and re-deposition is that now layer growth also takes place on the dome baffle where initially no Be flux and thus no Be layer deposition was occurring at all.

The second model calculation of T co-deposition in the divertor, using ERO, simulates the erosion and deposition along the inner and outer divertor graphite target plates (no W sections) in ITER. [7,5,63] A uniform beryllium influx of 1% (relative to the incoming deuterium ion flux) to the inner, and 0.1% to the outer, divertor has been assumed which is in agreement with the average values from DIVIMP as well as the high flux empirical estimates of section 3.3. Here we present a subset of ERO calculations presented elsewhere. [5,63] A homogenous mixing model is used. However, it has been found that applying a TriDyn-based model instead does not change the results significantly. Plasma background parameters such as temperature, density and parallel flow velocity from B2-Eirene (so-called case 585) have been used as input for these ERO calculations. [63] The B2-Eirene case 585 delivers deuterium ion fluences of $2.5 \cdot 10^{24}$ D^+/s at the inner and $4 \cdot 10^{24}$ D^+/s at the outer divertor target. Deuterium atoms (of similar fluence as ions) are taken into account in the ERO modelling to calculate the erosion of the divertor plates. The ERO modelling considers chemical erosion of carbon according to a yield Y_{Roth} depending on surface temperature, ion energy and flux. [64] Chemical erosion of deposited carbon is assumed to be ten times higher than Y_{Roth}. The sticking of hydrocarbons returning to the surface is assumed to be zero. Both effects together (enhanced erosion of re-deposited carbon and zero sticking of hydrocarbons) represent an enhanced erosion of in-situ growing carbon layers. [7] Sticking of beryllium and carbon atoms is determined by TRIM reflection coefficients. The assumed surface temperature profiles represent average operation conditions and lead to a maximum temperature of ~565 K at inner and ~1080 K at outer target plate. [65]

The ERO modelling results in large amounts of re-deposition of eroded particles on the target plates: nearly 100% for beryllium and 98 - 99% for carbon. Particles not deposited on the targets leave the simulation volume in the direction of the private flux region and are not treated by ERO anymore. It is assumed that these particles form layers at remote areas of the divertor.

Whereas in [7] constant values of (T+D)/C and (T+D)/Be in deposits have been assumed, here fit formulae based on experimental data are applied (equations 3.4.1-3) for layers deposited

on the targets. [23] The tritium content, according to these observations, depends on ion energy E_i [eV], surface temperature T [K] and in case of beryllium deposits also on the flux ratio $((D+T)/Be)_{flux}$.

These formulae are provided for certain intervals of energy, temperature and flux ratio. However, within the ERO modelling the values of these parameters along the ITER divertor plates can be outside these intervals, which can lead to unphysical tritium contents. Therefore an upper value of (T+D)/C = (T+D)/Be =1 is used. Using the beryllium deposition profiles from ERO together with profiles of surface temperature and deuterium impact energy results in profiles for (T+D)/Be and (T+D)/C as shown in figure 6.1.2 for inner and outer divertor. The red dashed line indicates a fuel ratio of 0.1 as has been used for beryllium and carbon layers in [7]. Also included in figure 6.1.2 are the modelled profiles of beryllium and carbon deposition rates. Taking these deposition rates together with the calculated (T+D)/Be and (T+D)/C finally results in tritium retention rates on the targets as summarized in table 6.1.2. For comparison the retention rates assuming fuel codeposition concentrations of (T+D)/Be = (T+D)/C = 0.1 are also included. As can be seen the overall tritium retention on the targets calculated with spatially resolved fuel ratio decreases from 7.1 to 1.9 mg T/s compared to the estimations using constant fuel ratio of 0.1. Generally, the tritium retention in beryllium layers decreases whereas the one in carbon layers increases. As for the previous calculations in [7], the main tritium retention takes place in beryllium layers at the inner target due to the assumption of a ten times larger beryllium influx to inner than outer divertor. This results in the overall decreased retention rate. For this set of data the total tritium retention amounts to 3 mg/s, or 300 g in 10^5 seconds.

A simple estimation (upper value) of tritium retention in remote areas assuming (T+D)/Be = (T+D)/C = 1 delivers an additional retention of 2.1 mg T/s and thus an overall retention rate of 4 mg T/s in beryllium and carbon layers at the targets and remote areas.

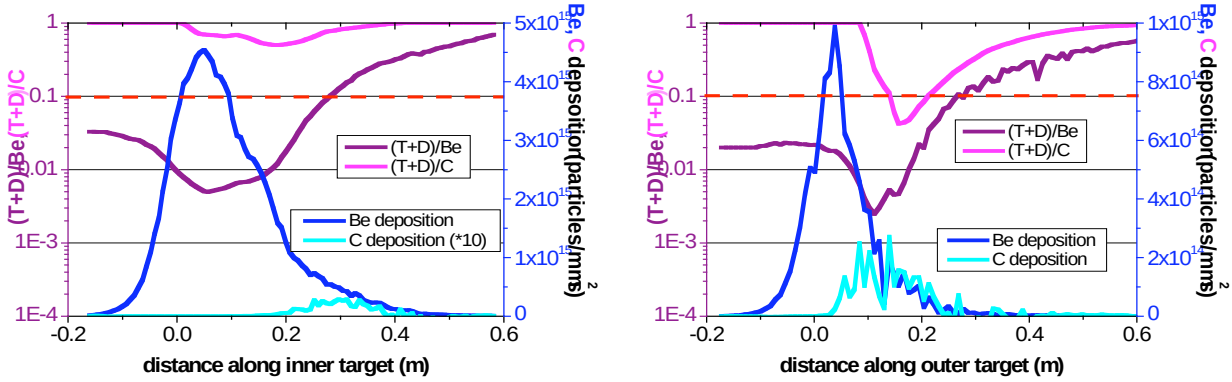

Figure 6.1.2: Calculated profiles of (T+D)/C and (T+D)/Be along inner (left) and outer (right) divertor plate. The red lines indicate the value as used in [7] for layers deposited on the targets. Also shown are the deposition profiles for beryllium and carbon as modelled by ERO.

	Divertor				**Remote**	
	Be		**Carbon**		**Be**	**Carbon**
	(D+T)/Be=0.1	**(D+T)/Be~fit**	**(D+T)/C=0.1**	**(D+T)/C~fit**	**(D+T)/Be=0.1**	**(D+T)/C=0.1**
Outer	0.9 mg T/s	0.17 mg T/s	0.2 mg T/s	0.29 mg T/s	0.02 mg T/s	0.8 mg T/s
Inner	6.0 mg T/s	1.3 mg T/s	0.02 mg T/s	0.16 mg T/s	0.1 mg T/s	0.1 mg T/s

Table 6.1.2: Estimated tritium retention rates for ITER on outer and inner target. Red values correspond to constant fuel ratios as assumed in [7], green numbers result from the usage of spatially resolved fuel ratios as obtained from equations 3.4.1-3.

Summing the information from Table 6.1.2 we see that the total retention ranges from 8.12 to 2.94 mgT/s, the range corresponding to the assumption of the incoming Be ion flux [(D+T/Be =1 vs. (D+T)/Be = fit). The contribution of remote regions (1.02 mg/s), based on the assumption stated, contributes between 12.5% and 35% of the total retention. If the C was removed (replaced by W) then this calculation at first glance indicated that the retention would drop to a range 6.82-1.59 mg/s, again the range is due to the different assumptions of the incoming Be flux. That corresponds to a 16% - 46% drop in T retention, so less than a factor of 2. Thus in our initial assessment of the effect of completely removing C from ITER the effect is not large, well within the uncertainties of the underlying physics.

Further ERO calculations are planned to analyse the influence of the assumption of enhanced erosion of re-deposited carbon and zero sticking for hydrocarbons. Also, plasma parameters from a new B2-Eirene run (so-called case 1084) will be used. Finally, more realistic beryllium influx profiles and concentrations will be addressed.

Concerns: Certainly the wall source calculation, both empirical and through DIVIMP, needs to be improved with better experimental measurements of the erosion, better measurements of the re-deposition in the main chamber. Of course we need better models of SOL flows to enable that as well. As pointed out earlier for the empirical calculation we also need better estimates of what fraction of the divertor erosion ends up in shadowed regions and what the characteristics of such co-deposited materials will be. Overall the modelling and empirical scaling projections of retention have to be made more consistent in terms of their assumptions and models.

6.2 Empirical projection of T retention in ITER assuming that all retention is due to T-C co-deposition in the divertor due to erosion from all-C walls, (A. Kallenbach)

As in Section 6.1a the method of estimating this quantity was strictly empirical, under the assumption that main chamber erosion is the source of C co-deposition at the inner divertor. It ignores erosion of the C divertor (and thus the associated co-deposition). The implantation into the full W divertor is ignored but can be obtained by looking at the second material combination – 6.3.

The assumptions of the material flow to the divertors together with surface temperatures and the corresponding co-deposition values are used to calculate the co-deposition rate at each inner divertor grid element. Then we integrate over the divertor to obtain the following:

κ= 150 W/(m-K)

Case	Inner div. retention	Outer div. retention	Total in 10^5s
Low wall flux	$3.07\text{x}10^{20}$ T/s (1.53 mg/s)	$4.2\text{x}10^{19}$ T/s (0.20 mg/s)	174g T
High wall flux	$1.53\text{x}10^{21}$ T/s (7.67 mg/s)	$2.1\text{x}10^{20}$ T/s (1.0 mg/s)	871g T

κ = 50 W/(m-K), hotter targets:

Case	Inner div. retention	Outer div. retention	Total in 10^5s
Low wall flux	$1.08\text{x}10^{20}$ T/s (0.54 mg/s)	$1.67\text{x}10^{19}$ T/s (0.08 mg/s)	63g T

High wall flux	5.41x10^{20} T/s (2.7 mg/s)	8.34x10^{19} T/s (0.42 mg/s)	313g T

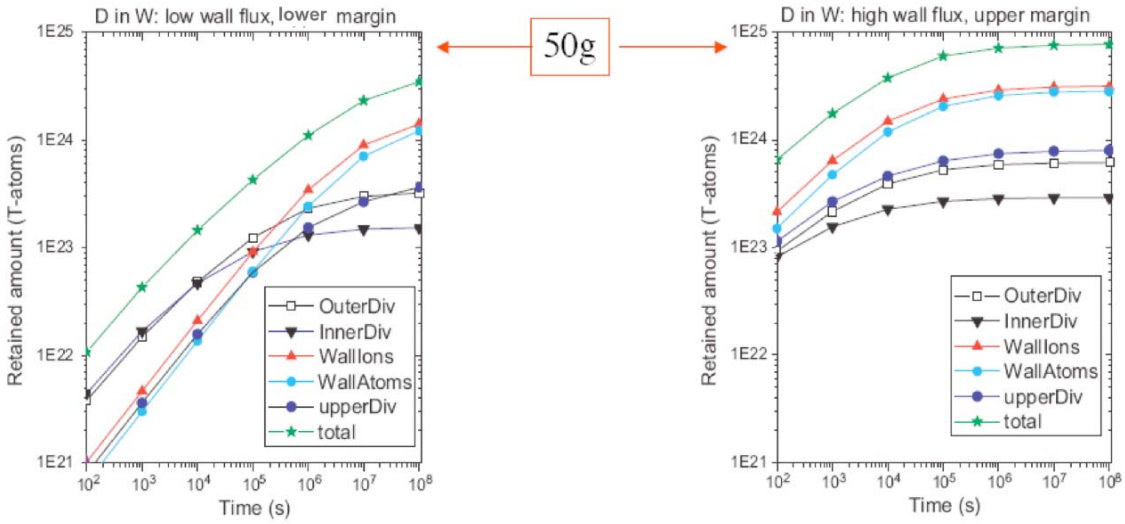

Figure 6.3.1: Retention of tritium in tungsten plasma-facing components. Left figure shows the low wall flux case with lower limit to the retention data (Fig. 3.5.1). The right figure shows the high wall flux case with the upper limit of retention data.

Overall, the retention of tritium by co-deposition with Be amounts to about 1/10 of the retention with C. As the erosion rates from the wall are assumed to be the same this difference is due to the much lower co-deposition efficiency under the assumed conditions, with the local surface temperature being the dominant parameter.

Concerns: Concerns are similar as for the empirical Be calculation (6.1a). Namely, we have poor knowledge of, or confidence in, the transport of first-wall material around the chamber to the divertors. We do not really know what the level of co-deposition is along the way.

6.3 All-tungsten PFCs in the case of no neutron damage (J. Roth)

An empirical projection of retention was also performed for all-W PFCs, with implantation, diffusion and retention in ion-induced or intrinsic defects in the W material being considered as dominant process. The same assumptions on wall and divertor fluxes and resulting surface temperatures were made as for the empirical projection for Be and C first-wall (Sections 6.1a and 6.2). From the range of retention data shown in fig. 3.5.1 the upper and lower fits were used for the evaluations and, as for C and Be, the two different wall fluxes, i.e. 1x10^{23} /s and 1x10^{24}/s, were assumed. The breakdown of the various regions in terms of fluxes (ions and neutrals), areas, and surface temperatures are again given in Appendix B).

Figure 6.3.1 shows the projected tritium inventories in different W PFC regions as a function of exposure time for the extreme cases: lower wall flux for the lower data fit limit of Fig. 3.5.1, and higher wall flux for the upper data fit limit. Due to the saturation inherent in the limit formulae of Figure 3.5.1 the retention also saturates. The largest amount of retention is at main chamber PFCs (low T_{surf} and large area). The projection to 10^5 seconds gives 3-30g T retained (low to high flux limit), the saturation retention in both cases is around 25 to 50g (lower to upper margin).

Clearly, the lowest retention was found for low wall flux and the lower limit of the data from Fig. 3.5.1, the highest for the high flux case and the upper limit.

Concerns: Most of the issues associated with this calculation are due to the underlying data for retention and as such were already covered in section 3.5. But we would like to mention again the concerns about saturation – what will the ultimate level be and at what fluence will it occur? In that regard the reader should also compare these results with those of section 6.5.2 which are based on just modelling assuming no saturation (Figure 6.5.5).

6.4 Summary of projections for non-neutron-damage operation

In the previous sections we have made projections using a number of methods and materials combinations. Here we try to bring them all together at one point in ITER operation, 10^5 seconds (250 400 second discharges), and with the same units.

PFC combination	Study	Wall retention included	Grams T retained
All-carbon	Kallenbach (empirical)		63-870
Be wall, C/W divertor (but no role)	Kallenbach (empirical)		4.1-82
Be wall, C divertor	Kirchner (ERO+ empirical/Divimp)		294
All-tungsten	Roth (empirical)	X	2-29

Table 6.4.1: Compilation of projections for non-neutron-damage scenario. All projections include retention in the divertor. Only one takes into account retention at main chamber surfaces.

At 10^5 seconds all-carbon or Be wall + carbon divertor all lead to significant retention in the divertor PFCs. The all-W case is lower than the range of almost all the predictions for other materials. Beyond 10^5 seconds the tungsten, based on the saturation effect implied by laboratory data, would tend to saturate. On the other hand the Be and C co-deposition would be expected to be linear in time. Allowing for co-deposition in the main chamber would certainly increase the projections for that material but the amount is difficult to estimate given our poor knowledge of erosion, transport and deposition in the main chamber. If, on the other hand, the divertor CFC surface were replaced by W we only expect a factor of order 2 drop in the divertor co-deposition, far smaller than the uncertainties in other aspects of the calculations.

6.5 Retention for all-W PFCs with neutron damage effects

6.5.1 Analytic evaluation of T retention (R. Kolasinski, B. Lipschultz, W. Wampler, D. Whyte)

Based on the models discussed in Section 4.2 we have made analytic projections to ITER of the effect of neutron damage on T retention under the assumption of constant traps at the full lifetime ITER limit – 1% of the W density, 6.5×10^{28} m^{-3}. This calculation is only to be viewed as a guide and a check on more detailed numerical calculations as this analytic model assumes the traps are

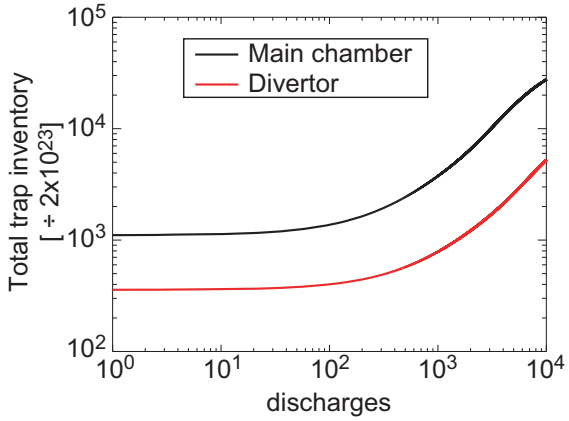

Figure 6.5.1: Logarithmic version of Fig. 4.1.2: total traps (for D+T) including both intrinsic and those from neutron damage vs discharge for full power, Q=10, ITER discharges. The number of traps are divided by $2x10^{23}$.

filled with T as the traps appear due to damage - obviously an overestimate given it does not take into account the time it takes for the hydrogen to diffuse to the traps. The model used here assumes neutron damage rates ($0.5x10^{-7}$ dpa/s for the divertor, $1.0x10^{-7}$ dpa/s for the main chamber) together with the conversion of that damage to traps (Fig. 4.1.1 and accompanying equations). We again plot in Figure 6.5.1 the total D+T trap sites in the main chamber and divertor (given in grams) under the assumption that 50% of all available traps are filled with T, the rest with D. This calculation further assumes 1 cm tile thickness, 680 m^2 of main chamber and 220 m^2 of divertor area. Note that it is of order a few 100 discharges before the nuclear damage doubles the intrinsic traps in the bulk.

As can be seen from Figure 6.5.1 the main chamber will dominate in terms of the number of available traps. That is of course due to its area, ~ 3x that of the divertor.

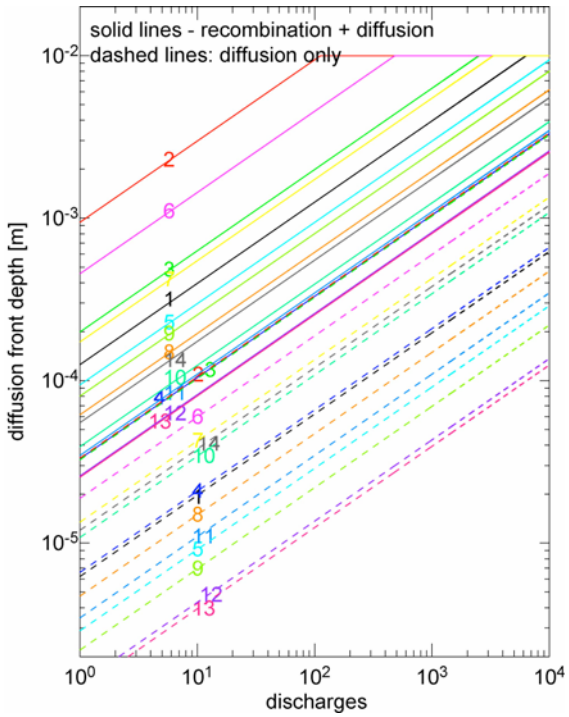

Figure 6.5.2: Diffusion front depth for 14 regions defined in Appendix A. Constant trap density of 1%W is assumed.

One can ask how deep into a tile the tritium must reach and fill 1% trap concentrations before ITER reaches the 700 g limit. Assuming the total ITER area of 900 m^2 that depth is 0.48 mm. If only the divertor is tungsten the depth is ~ 2 mm.

The analytic formulation in section 4.2 gives the rate at which tritium permeates to the traps as determined by a combination of the diffusion coefficient (so local temperature) and the near surface concentration of mobile D in interstitial solution sites, which drives the implanted D down the concentration gradient into the material. The near-surface concentration depends on temperature, incoming flux, and loss at surfaces and other near-surface sinks such as internal cavities or bubbles. Using the analytic model of section 4.2 we can calculate the depth that the diffusion front reaches vs time or # of 400s ITER, Q=10, discharges. The result is shown in Figure 6.5.2 for the 14 regions described in Appendix 1. Regions 1-4 correspond to the outer divertor, 5-8 the inner divertor, and 9-14 the various main wall surfaces. The diffusion front location for each of the 14 regions is shown twice, once for the front surface density determined by diffusion only (infinite recombination), and secondly for the case where the recombination dominates (recombination level as specified by the results of Wright for Mo [29]). Note that in the recombination dominated case the diffusion front reaches the back of the tile (.01 m) before the 10^4th ITER discharge for regions 1-3 as well as 5-7, all in the divertor. The affected area is small, ~ 20 m^2.
The surface densities are ~ 1000x higher in the recombination-dominated case. Increasing the recombination rate a factor of 10^5 over that found by Wright, to a level similar to that determined by Anderl [57], essentially eliminates the surface density enhancement over that of diffusion only. Such an increase is much less than the range of 10^{20} in model and measured recombination rates discussed in section 4.2

The effects of low surface recombination rates and the dominance of the main chamber are also evident when examining the actual T that is projected to be retained. Figure 6.5.3 displays the sum of T (taking into account D fills half the sites) retained if all neutron-induced traps are filled up to the depth of the diffusion front of Figure 6.5.2 assuming a 1% trap density constant in time. Integrals over the 14 regions - inner and outer divertor as well as all main chamber - have been done. Of the main chamber regions the contributions in order of dominance are regions 11 (Wall between limiters), 10 (peak flux on limiters), 14 (Upper divertor), 12 (shadowed regions between limiters) and 13 (shadowed, from ions, regions). Of course region 11 has the largest area (315 m^2). We note that although the main chamber ion flux used in this case (high flux) is $1x10^{24}$/s, the neutral flux is over a factor of 2 larger than the ion flux. This is partly due to an assumption in region 12 of neutral flux being twice the ion flux (based on KN1D modelling). There are also several regions where there is no ion flux (regions 9 & 13) and the neutral flux is set to low values corresponding to pressures of $1.3x10^{-3}$ Pa at 5 eV neutral temperatures which is an average over those generated in the plasma through charge exchange and those corresponding to Franck-Condon dissociation. Even so the total neutral fluxes are large given the large areas.

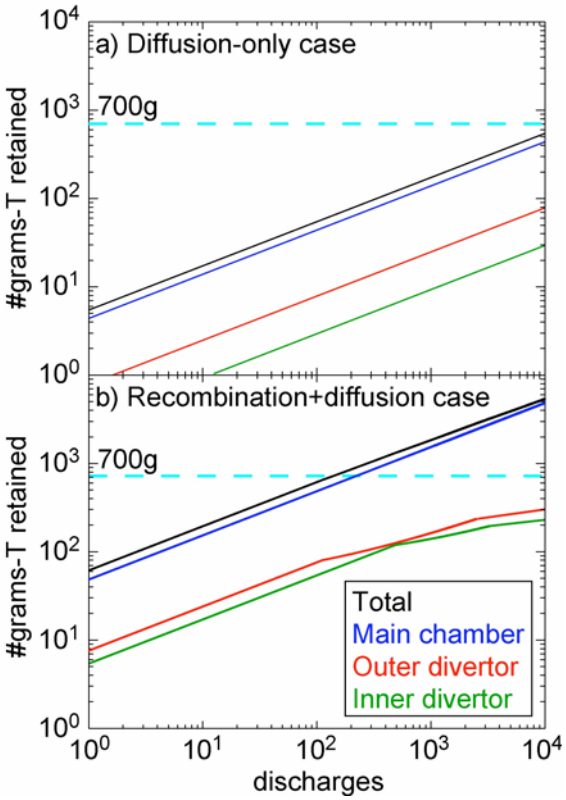

Figure 6.5.3: Amount of tritium stored in neutron-induced + inherent traps for a) diffusion-only cases; and b) recombination + diffusion. ***Constant trap density of 1%W assumed.***

Note that the effect of the diffusion front reaching the back of the tile is evident in the 'saturation' in a number of areas shown in Figure 6.5.3.

We can gain some insight into the time-dependent effect of the neutron-damage sites over the inherent trap level, set to .05% of the W density. Figure 6.5.4 displays the same analytic derivation of the total retention given by Figure 6.5.3 for the diffusion- and recombination-dominated cases along with 2 other limits: 1) no enhancement of traps due to neutron damage (so the trap level is kept constant at .05%W) and 2) the enhancement of traps following the prediction of Figure 6.4.1. Allowing for changing trap densities is physically incorrect as it assumes that the trap filling is independent of the T diffusion which it is not. So the three calculations are really just meant to give the reader an intuitive feel for what to expect from the modelling which follows in the next sections. But generally one can conclude that the enhancement of the trap density by a factor of 20 has a $20^{0.5}$ = 4.5 increase in retention during the period of ITER operation. Also, the effect of neutron-induced traps would not be significant until of order 1000 Q=10 discharges are reached.

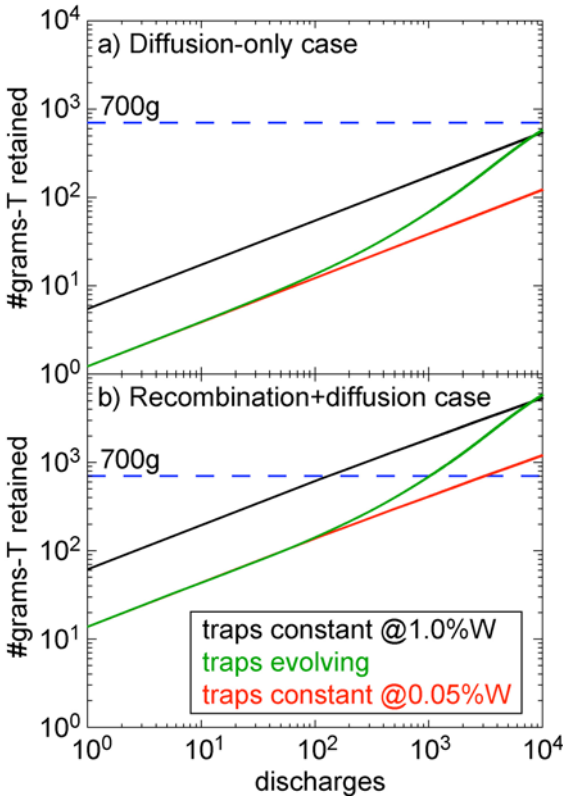

*Figure 6.5.4: Same as Figure 6.5.3 but showing, in green, an approximation for the effect of **traps increasing in time**: Amount of tritium stored in neutron-induced + inherent traps for a) diffusion-only cases; and b) recombination + diffusion. The different time dependence corresponds to the three cases of constant traps (1%W and .05%W) as well as traps increasing with time from Figure 6.4.1)*

follow. It is not meant to be quantitatively accurate as it ignores de-trapping and does not properly treat the role of traps increasing with time and it ignores several effects including de-trapping and annealing of damage. Furthermore, near-surface precipitation, which has been observed to occur, will reduce the rate of D permeation to greater depths, and this effect is also neglected here. In general the main concerns for such calculations are: a) the accuracy of the conversion of dpa to traps, which depends on temperature because of damage annealing, b) the concentration of mobile D produced near the surface by exposure to the plasma, c) the binding energy of D to the traps, and other such issues as described in sections 4.1 and 4.2.

It is interesting to compare the projections for T retention based on the analytical formulation, for inherent traps and no surface recombination effect, with the projection to ITER based on the laboratory data scaling of Figure 6.3.1. At the 10,000 discharge point the diffusion model data *with no neutron-damage* of Fig. 6.5.4 lead ~ to the same levels as the projection shown in Fig. 6.3.1. **IF** one assumed that the experimental formulation underlying Fig. 6.3.1 is 'truth' then the implication is we should ignore the recombination-dominated projections of Fig. 6.5.4. However, as discussed earlier, we should not ignore the potential for recombination effects to be significant in the tokamak, as opposed to laboratory, setting.

Concerns: This section is really meant as a guide to assessing the modelling results that

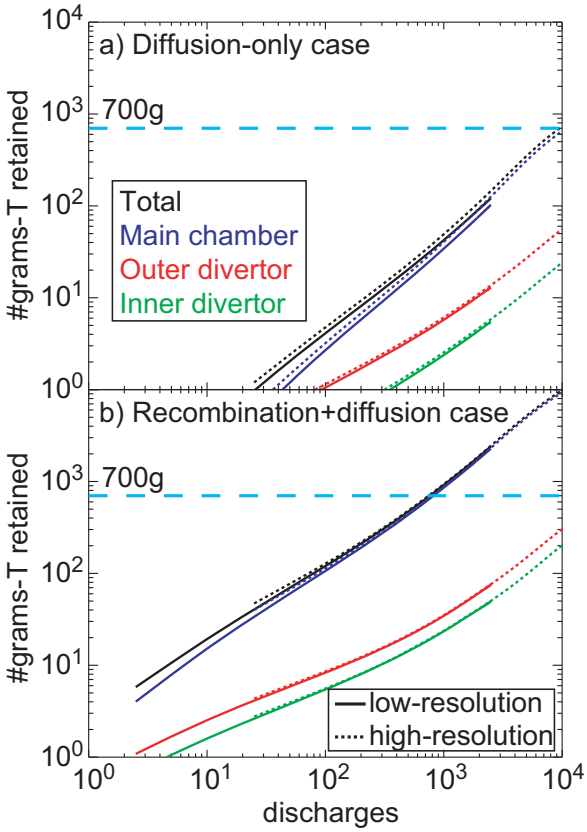

Figure 6.5.5: Results of the WW code projection of T retention in neutron-induced + inherent traps for a) diffusion-only cases; and b) recombination + diffusion. The solid lines correspond to the low and high resolution cases respectively.

6.5.2 Model projection of T retention (D. Whyte, R. Kolasinski)

Having made a number of empirical projections to ITER in the previous sections we now turn our attention to the predictions of retention in W based on two currently available hydrogen transport codes. As described in Section 4.3 and Appendices C and D the two codes used in this study, WW and TMAP, have been benchmarked and adjusted so that their results are fairly close. The primary issue that remained after the comparisons of Appendix D was that the time steps and grid spacing of WW were too coarse for short time scale predictions. To address this concern WW was run on the same input conditions twice for each of the 14 regions of T implantation – 'high resolution' (small grid spacing and time step) and 'low resolution' (larger time step and grid spacing). The results **for the high flux case only** are shown in Figure 6.5.5. The effort to run the code for the low wall flux case was not deemed warranted; it would result in a simple shift of wall retention to one order of magnitude higher numbers of discharges while the divertor retention stays constant. As was found earlier for the lab-based (Fig. 6.3.1b) and analytic (Fig. 6.4.4) high-flux case projections the amount retained for less than a few hundred discharges scales with fluence to a power of order 0.5 (different for the Fig. 6.3.1b and 6.4.4). In addition, all projections show that the main chamber would be the primary region of retention due to the large area. After a few hundred discharges the lab-based projections (Fig. 6.3.1) saturate as assumed in the fits to the data (Fig. 3.5.1) while the analytic and WW model projections actually are enhanced due to the effect of neutron traps (absent in the lab-based projection, Fig. 6.3.1).

6.5.3 Summary of retention in an all-W ITER and concerns

There is a wide range of projections for retention in an all-W ITER. For the lifetime of ITER (10000 discharges) the lowest projection of 5-10gT is for no neutron-damage sites, low wall fluxes and saturation of retention (Figure 6.3.1a). If the neutron-damage sites are **not** accessible by the T (e.g. diffusion barrier near the surface or trap annealing) then the maximum we might expect would be in the range of the high wall flux limit projection of Fig. 6.3.1b and 6.5.4 (red line), of order 100g over the lifetime of ITER. That number is of course limited by the assumption of saturation of retention (Fig. 6.3.1b). Relaxing the assumption of saturation in retention and allowing access of the T to the neutron damage sites raises the high wall flux case T retention projection from 50 to ~ 700g over the ITER lifetime (diffusion only case, Figure 6.5.5a). A further potential increase in retention would occur if the recombination rate at the front surface was low enough, thus raising the T density there and driving it into the bulk faster (Figure 6.5.5b). The 700g limit would then be reached at close to 1000 discharges. Conversely, near-surface precipitation may reduce the permeating flux [33,49] and the retained quantity of T below the 700g lifetime retention prediction of the diffusion only case. The bottom line is that even under the most conservative assumptions an all-W ITER could operate for ~1000 full performance discharges before reaching a limit in in-vessel T inventory (Fig. 6.5.5b).

Such a wide range of projections is reasonable given the state of our understanding. Certainly among our group we cannot agree on the probability of all of the above scenarios. Again, the reader can assess the various projections based on the source of assumptions. Our group does feel that several areas of research would serve to reduce uncertainties and the range of projections. Those areas include the actual level of wall fluxes as well as the retention of T in W under simultaneous T, He, impurity and neutron bombardment. Simultaneous implantation by the various species is needed to evaluate a) whether the simultaneous implantation (at the right range of fluxes) somehow synergistically reduces the retention, b) whether the H implantation somehow enhances the density of surviving neutron damage sites (e.g. by H filling damage sites before they can recombine). It is doubtful that such exact simulations of

ITER can be done before ITER operates but various aspects of such situations can be studied in isolation and hopefully, with physics understanding, combined to better project to ITER.

7. Underlying uncertainties, assumptions and future work

In the course of this study a number of areas were identified for further research either because they were not included, or because the level of understanding is very poor. In the numerous steps between main chamber source and final co-deposition the first uncertainty is in the first-wall fluxes including their characteristics (energy of ions and neutrals) and flux pattern. Secondly we have a difficulty of how to split up a general prescription for radial fluxes (and localized erosion) amongst the various 3D objects in the SOL including limiters and tile gaps. We need to better understand the transport of eroded material from where it is eroded (first-wall or divertors) to where it finally re-deposits and possibly co-deposits. This includes the local physics of erosion and re-deposition (and co-deposition) as well as the continual re-erosion and migration of material as it moves along the first-wall, probably co-depositing with T in remote areas along the way to the inner and outer divertors. Certainly much of the above could be addressed with a better understanding of parallel and perpendicular plasma transport for the fuel ions and impurities. A significant unknown is the effect of transient heating (ELMs and disruptions) which could lead to both reduced retention (increased temperatures) and enhanced retention (spread co-deposition to cooler areas), both at the divertor plates and elsewhere.

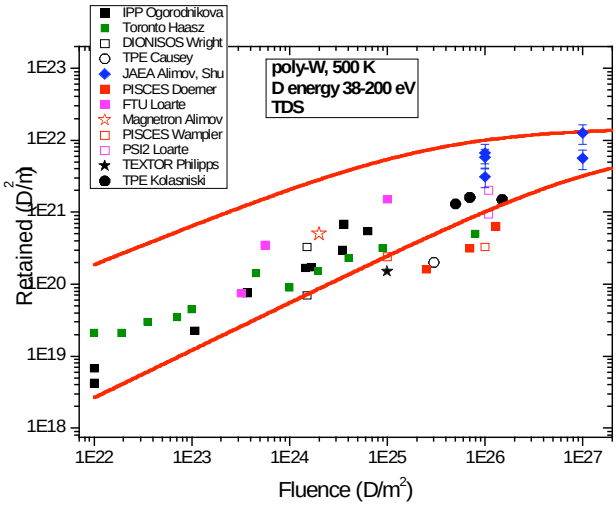

Figure 7.1.1:Version of Figure 3.5.1 with new data from U. Toronto and Alimov added.

In this study the range of possible material properties for Be and C were not really taken into account. Any follow-on study should undertake to set a range of erosion rates for each material. In addition the properties of the re-deposited material, in terms of T retention, need to be addressed for how the retention changes as a function of material temperatures, both for steady state and for transients such as ELMs. There is new data for the effect of baking following co-deposition with and without mixed materials presented at the December 2009 ITPA SOL/Div meeting in San Diego by J. Roth.

With respect to W the uncertainties are more related to what happens in the material as opposed to in the plasma: The exact nature of T accumulation in the region of the implantation depth through expanding or creating traps is uncertain. Likewise, when T agglomerates into voids or bubbles we need to quantitatively predict what the effect on retention locally is (whether the T is trapped or released through rupture back to the surface) and whether such material structures impede diffusion and trapping of T further into the bulk. In other words given all the obvious changes in micros-structure and composition of the near surface what are the related effects on diffusion to greater depths? There has been recent work on the issue of surface modification by the IPP-Garching and JAERI groups [66-68,54] showing near-surface damage structure at high fluence (10^{26}/m^2 - 10^{27}/m^2) that appears responsible for release of D and corresponding saturation in retention. A study of ideal (e.g.

non-tokamak) W [69] determined recombination rates at the front surface in line with those from Anderl[57] and Baskes[70] (section 4.2).

In the area of retention as a function of fluence on W there have been some additions/changes to Figure 3.5.1. First, new low energy data (200 eV) from Univ. Toronto [71] replaces the earlier, higher energy ion data [24]. These new results extend the fluence range previously obtained with ion beams by an order of magnitude, to ~10^{26} D/m^2 (up to the fluence range of plasma devices), and confirm the power-law dependence of D-in-W retention on D fluence over this extended range. The new results also agree well with similar results from IPP. Secondly, additional data from the same study by Alimov at high fluence were added[31]. The new points have slightly higher retention but are similar in trend. Most of the old data along with the new are shown in Figure 7.1.1. The old upper and lower guidelines used for this report are shown as well. Certainly any new study should take these changes into account and possibly adjust limits. The question of how to handle saturation is particularly important as illustrated earlier in section 6 where the empirical scaling (Figure 6.3.1) is compared to the modelling projection to ITER (Figure 6.5.5).

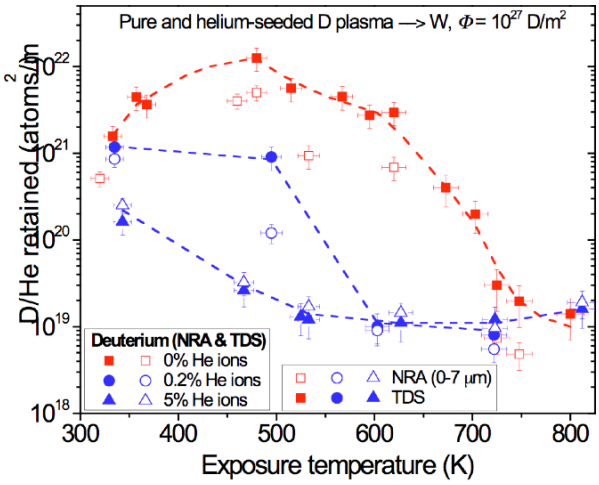

Figure 7.1.2:Example of the reduction in H retention with addition of simultaneous He+ implantation from Alimov et al.

At the beginning of this study the characteristics of traps created by nuclear damage (trap energy, de-trapping rates, trap density, the T/W enhancement over undamaged W) were very uncertain. The efforts to deduce the level of T retention from the little data available shown in this report turn out to be consistent with the follow-on data that was obtained this last year by a number of groups [72-74,49]. In addition the same data shows retention in damaged material dropping strongly with increasing temperature[72,74,49]. However, more experiments are needed to clarify the rate at which damage-induced traps are filled and hence the depth to which trapping extends into the material with the corresponding enhancement in T inventory.

Lastly, there is evidence that impurities can play a role in affecting T retention. Certainly we have discussed earlier the effect of impurity implantation on retention. But in the past year there has been surprising unanimity amongst a number of laboratories in finding that simultaneous implantation of He and T ions at low He concentrations (less than ~ 5%) lead to dramatic drops in T retention, up to a factor of 1000[31,66,75-79,49]. An example is given in Figure 7.1.2. Some decrease in retention due to simultaneous He/H ion implantation is also found for nuclear-damaged material [49].

8. Conclusions

As can be seen from reading the details of this paper, the exercise of bringing together all the processes connected to retention is very complicated and involves processes which currently have very large uncertainties (e.g. impurity transport). The range in the projection for a given material or situation does not represent the underlying uncertainty (or error bars) but a range of conditions that we deem ‘probable’ at this point in time. In fact, for a number of parts of

this analysis (e.g. the level of erosion and finally co-deposition at the inner divertor) we are making educated guesses.

What is clear from this research effort is that our current understanding leads to the conclusion that a fully carbon first-wall will probably lead to higher T retention than for a Be first-wall due to a combination of factors:

1) Lower T/Be than T/C for a given temperature and incident impurity flux fraction (Γ_{imp}/Γ_{D+}) incident on the final co-deposition surface; and

2) The higher probability of C to migrate to remote areas due to the form of its chemical erosion products.

The analysis of the various scenarios included in this report also informs the debate on the T retention difference between the standard Be/W/C configuration and the Be wall, all-W divertor. The ERO analysis, as well as the discussion of co-deposition properties for Be and C, both point towards a minor drop in T retention, less than a factor of 2 in the changeover due to the fact that the main source of retention, T co-deposition with Be, has not been removed. Of course the T in Be co-deposits is easier to thermally remove than T co-deposited with C. However the impact of material mixing has not been addressed in this report and may have a substantial effect on the release of T from co-deposits formed in ITER.

Furthermore, this comparison of material properties and performance indicates that, in the absence of nuclear damage, a fully-W first wall will probably lead to lower T retention than the standard ITER mix of materials (C/W/Be) or an all-carbon case.

The subject of nuclear damage, the trap sites created and how that leads to retention is subject to rapidly changing knowledge. Our initial analysis indicates a possibility of a high capacity of the damaged W to hold T. Based on this initial analysis it is still probable that tritium retention for an all-W machine would be lower than for the 2 other cases examined. Such retention would likely be lower still if surface recombination does not play an important role, if near-surface precipitation of the implanted T impedes its diffusion deeper into the bulk, and if thermal de-trapping and annealing of damage are taken into account.

The uncertainties of the above probable outcomes, as ill-defined as they are, are different for W than for C and Be. All processes leading to co-deposition of T with C or Be are uncertain. Such processes include the rate of erosion of from main chamber surfaces, the level of local re-deposition and co-deposition (e.g. on sides of tiles), the rate of migration around the vessel and how much is deposited (and co-deposited) along the way, the deposition pattern at the inner and outer divertor which should include how much finds its way to shadowed areas near the divertors.

The uncertainties for retention in tungsten are different in most ways. They include uncertainties in ion/neutral fluxes to main chamber surfaces as well as their energies. In general though the uncertainties for retention in W are for processes in the material – The exact nature of T accumulation in the bulk through expanding or creating traps is uncertain. Likewise, when T agglomerates into voids or bubbles, we need to know whether that impedes diffusion and trapping of T further into the bulk. And of course the characteristics of traps created by nuclear damage (trap energy, de-trapping rates, trap density, trap annealing) and the ease with which the implanted T can reach them need more research.

There are fundamental differences between the different materials in terms of how the T will be retained: Retention due to co-deposition with C and Be is a surface effect. Retention in W will be further into the bulk, potentially throughout the entire bulk. The implication is that co-deposition is amenable to surface heating/removal. Bulk retention is less amenable to T

removal (but possibly immobilized from the safety point of view). T removal techniques are required, but will likely be very different for Be/C and W. In all cases higher surface and bulk temperatures generally lead to lower retention.

In summary we advise readers to look at this work more as an identification of areas needing additional research, rather than a material selection recommendation. Use of this work to select, or deselect, one material compared to another, is not wise. In addition, issues such as component lifetime, dust, and the material's effect on the core plasma should be included in any material decisions along with T retention.

Acknowledgement:
We thank our many colleagues in the materials, SOL and divertor physics areas whose work this is based on.

Appendix A: Calculation of wall fluxes (A. Kallenbach, B. Lipschultz)

Utilizing the current database of tokamaks separatrix data we calculate first the SOL profiles expected for ITER (A.1). Those profiles allow us, with further assumptions to calculate the time-averaged heat flows to main chamber surfaces (A.2). Following that we utilize two methods to calculate the wall fluxes and energy characteristics of those wall fluxes (A.4, A.4).

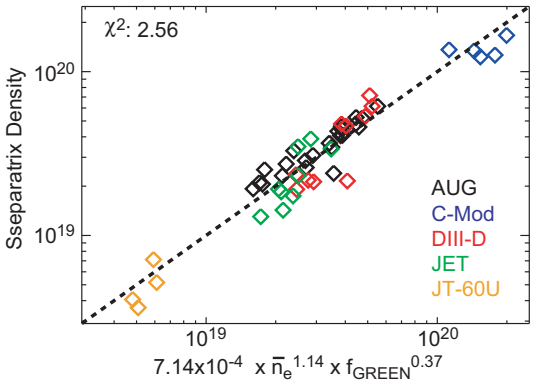

Figure A.1: Scaling of separatrix density across tokamaks.

A.1 ITER SOL profiles

We base the prediction of the SOL profiles on analysis of a multi-tokamak (C-Mod, DIII-D, ASDEX-Upgrade, JET, JT-60U) database of near-separatrix profiles. [80] From this a scaling of the separatrix density can be fit (shown in figure 1.1.1) which predicts separatrix density ≤ $4x10^{19}/m^3$. Similar values ($3\text{-}5x10^{19}/m^3$) are found on the basis of ITER modelling [81]. For this exercise we will use a value of $3.5x10^{19}/m^3$.

The same database was used to derive the density e-folding length, $\lambda_{n,sep}$ in the region of the separatrix - the so-called near SOL. The data are more scattered than for the separatrix density giving values in the range 40-55 mm. We note that ITER modelling gives ~ x2 smaller values. For this exercise we assume 50 mm.

For the purpose of calculating heat loads we also need the temperature profile. The same database provides us with values of $\lambda_{T,sep}$ ~ 2 cm. We limit Te at a low value of 10 eV in the far SOL. T_i is assumed to be $2xT_e$.

Together we display the profiles in Figure 1.1.2.

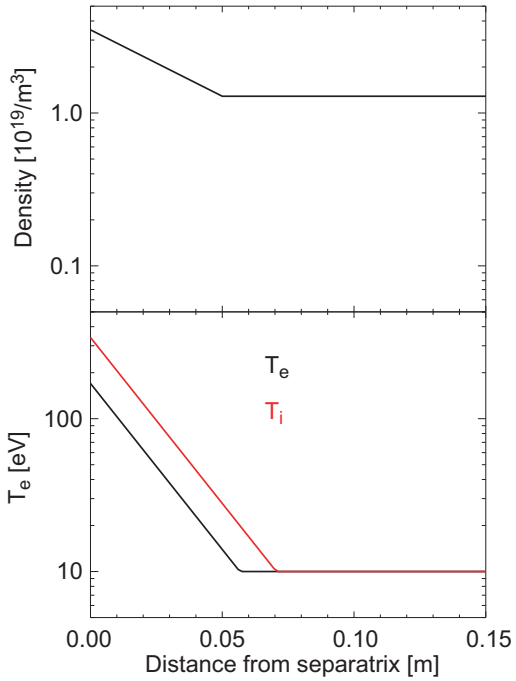

Figure A.2: Assumed steady state density and temperature profiles.

A.2 Upper divertor fluxes

To calculate the particle and heat fluxes to the upper divertor we need to make further assumptions:

- second separatrix (drsep) at 5 cm from the separatrix at the outer midplane;
- 20% of ELM energy (1 MJ) goes to upper divertor (and outer wall both). The second separatrix ELM density is $1x10^{19}/m^3$ and the separatrix temperatures adjusted to give 200 kJ/ELM (Te~ 300 eV, Ti~ 600 eV).
- ELM frequency 40 Hz, e-folding length for ELM power outside ssep = 5 cm
- Ti always $2xT_e$
- Midplane B_{Pol}/B_{Tor} ~ 0.35
- Outer midplane between ssep and limiter radius is 10 cm from 8.05 to 8.15 m.

This maps to upper divertor with x10 flux expansion from R=5-6m.

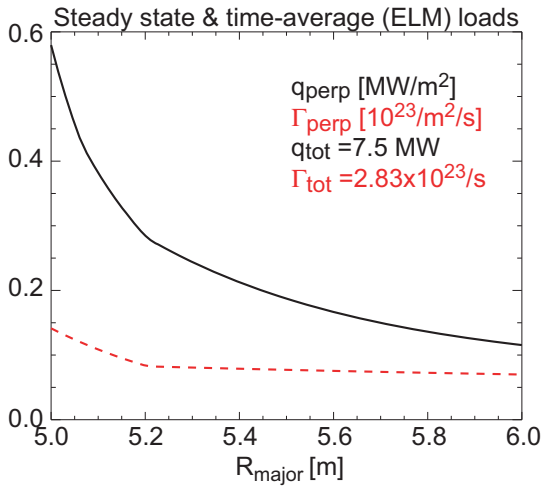

Figure A.3: Calculated steady state + time-averaged heat and particle flux profiles at the upper divertor

- Flux expansion from the midplane to the upper divertor ~ 10
- Coolant temperature 400K

The heat flux load is assumed to be free flow along the flux tube ($0.5nc_sx(2.0T_i + 2.0T_e + 3.5T_e)$) where the terms are the ion and electron thermal energies (half Maxwellian) and the energy gained in the sheath + pre-sheath. Since the actual geometry is not being used we take the parallel power flow and convert it to poloidal power flow:

The poloidal power flow is then mapped to the upper divertor according to the flux expansion and change in R in the assumptions. Taking into account the ELM and steady state particle and heat flows the resultant particle and heat flows to the upper divertor are given in Figure 1.1.3.

The 'normal', or time-averaged, loading to the upper divertor is fairly low – 7.5 MW and ~ $2.8x10^{23}$ particles/s. The corresponding peak heat load is < 1 MW/m^2 (time-average), with higher values during an ELM – 7 MW/m^2. These results are based on the assumption of 1 MJ ELMs at 40 Hz (10% going to upper divertor). The corresponding delta-T between surface and coolant will be small. Of course there are 'off-normal' loads as well as uncertainties on what ELMs will really be like.

Average surface temperatures range from 420K (high conductivity) to 470K. These are accompanied by average fluxes of $8x10^{21}$/m^2/s over 35 m^2.

A.3 Scaling wall fluxes from ASDEX Upgrade to ITER

Predictions for the ITER wall ion fluxes have been obtained by scaling from the total main chamber ionization rate in ASDEX Upgrade obtained by H_α spectroscopy. ASDEX Upgrade is in particular well suited for these scaling studies since it has similar separatrix densities compared to ITER and similar plasma shape and high heating power available. Different scaling assumptions have been used: a) Similar relative edge density profile shapes in ITER and AUG in combination with a diffusive transport ansatz, b) identical radial flux densities for similar values of P/R, where P is the total power through the separatrix and R the major radius; and c) the same exercise assuming flux density similarity for the same P/R^2.

With the diffusive ansatz using D= 3 m^2/s and an assumed density gradient of 2 10^{19} m^{-3} / 0.05 m, a flux density of 1.2 10^{21} m^{-2}s^{-1} was obtained. Taking into account the experimental observation that the outflux is concentrated around the outer midplane, a fraction of 1/3 of the ITER surface area of 680 m^2 is used resulting in a total inter-ELM outflux of 3 10^{23} ions/s. This ion outflux partly recycles on LFS limiters, a significant fraction is directed towards the HFS due to (~ parallel) SOL flows. For standard AUG conditions, the recycling flux on the HFS dominates the LFS value by typically a factor 2-4, depending on inner and outer wall

clearance. However, the flux densities are larger on the LFS due to the much smaller limiter wetted area.

Under the assumption of ion flux density being the same in AUG and ITER for similar P/R^2 we use from AUG a medium power discharge (7.5 MW and R= 1.65m, S=43 m^2) with total wall flux 2 10^{22} ions/s. ITER has 100 MW and R=6.2 m for P/R^2 of 2.6 (AUG value close at 2.75). Assuming the ion flux densities are the same then the total flux in ITER is obtained by multiplying the AUG value with $(S^{ITER}/S^{AUG}) = 16$ to account for different surface areas. This results in a predicted ITER wall ion flux of 3 10^{23} ions/s, similar to the diffusive ansatz. If P/R were the correct similarity parameter, the high ITER values cannot be achieved in AUG. So we take the measured AUG recycling flux and scale by its power dependence, which is roughly $P^{0.25}$ [82] from 7.5 MW to 26.6 MW which would be required to have the same P/R in AUG compared to ITER (a factor of $(26.6/7.5)^{0.25}=1.37$). We then can scale by the areas again (factor of 16) giving an ITER value 4.4 10^{23} ions/s.

Recent high power AUG discharges (12 MW, P_{sep}~10 MW) with higher current (1.2 MA) showed a total main chamber recycling flux of 10^{23} ions/s, including the effect of ELMs which carry about 33% of the time-averaged recycling. Extrapolating these values according to P/R^2 (again, assume the same scaling with area of x16) suggest an ITER inter-ELM recycling level of $1.1x10^{24}$ ions/s or $1.6x10^{24}$ ions/s if the ELMs are taken into account. No power scaling is used here, the AUG P/R^2 is higher and the AUG P/R is lower than the ITER value.

Taking the average of the different methods, a total inter-ELM recycling level of 7 10^{23} ions/s is recommended, and 1 10^{24} ions/s regarded as upper limit.

The in-out asymmetries depend on the respective wall clearance and probably also the number and shape of the limiters. In AUG, a major part of the flux recycles at the high field side, but approaching a double-null configuration, a part of the parallel flux directed to the HFS is expected to be directed towards the upper divertor. The following distribution of the total ion wall flux Γ_i is suggested: $1/3\Gamma_i$ to the LFS, $2/3\Gamma_i \exp(-dR_{XP}/\lambda_n)$ to the upper divertor and $2/3\Gamma_i (1 - \exp(-dR_{XP}/\lambda_n))$ to the HFS. dR_{XP} is the distance between the two X-points mapped to the outer midplane and λ_n the density e-folding length (~ 50 mm).

A.4 Convective model scaling of wall fluxes to ITER

This method assumes that the far SOL transport (radial flux of ions, Γ_{radial}) is dominated by convection, $\Gamma_{radial}= nv_{eff}$, where v_{eff} is the convective velocity. Based on analysis of multi-tokamak (JET, DIII-D and C-Mod) L-mode similarity discharges it was found that the far SOL convective velocity was essentially independent of dimensionless parameters (ν*, ρ* and β) [83,84]. Examination of H-mode plasmas led to similar levels of wall ion fluxes as found in L-mode [85]. The implication for ITER was that far from the separatrix (limiter radius, r/a~1.08) a convective velocity range of 50-100 m/s would be predicted. A value of 75 m/s was selected for this exercise.

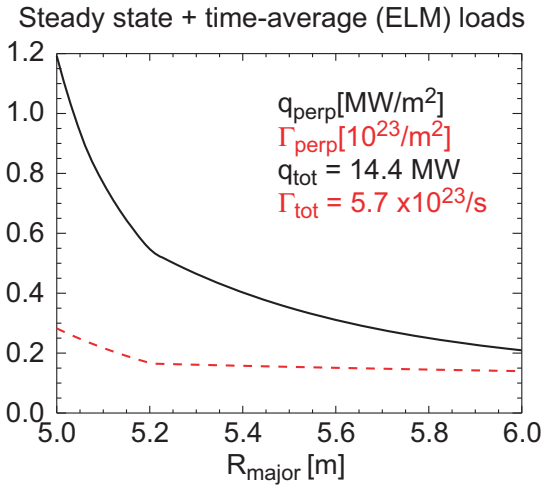

Figure A.4: Calculated steady state + time-averaged heat and particle flux profiles at the upper divertor

Based on the convective paradigm and the SOL profiles of section 1.1.1 we can make predictions of the ion flux reaching the main chamber surfaces. The limiter density from the Figure 1.1.2 density profile is $1.3x10^{19}/m^3$. Together with 75 m/s the time-averaged flux would then be $\sim10^{21}/m^2/s$. Over the 670 m^2 of vessel surfaces (excluding the divertors) that leads to a total flux of $\sim7x10^{23}/s$. As part of this study we compared the L-mode and H-mode (with ELMs) particle fluxes to the main chamber surface in DIII-D based on work by Leonard. [85] The fluxes were essentially the same after taking into account ELMs.

The power fluxes to main chamber surfaces are more difficult to estimate in light of the ITER specification of ELMs with < 1 MJ energy losses. First, examining only the steady state heat flux it is simply the wall flux ($7x10^{19}$) which carries (2Ti + 5.5Te) per ion-electron pair (~ 100 eV), or 11 MW. If we utilize the densities and temperature profiles for ELMs discussed earlier, together with an assumption of 75m/s convective velocity, we find that the instantaneous energy carried by each ELM at the limiter radius to be ($1x10^{18}/m^3$ x 500m/s (assumed for ELMs) x 2000eV/ELM x $1.6x10^{-19}$ J/eV x .001s/ELM x 670 m^2) ~ 100kJ or 4.2 MW averaged over time. So ~ 15 MW to the first wall other than divertors.

We can sum the upper and divertor particle fluxes. Together with the upper divertor flux ($2.8x10^{23}/s$) the total wall flux would be $\sim1x10^{24}/s$. The total power to all surfaces outside the lower divertor would be 15 MW (main chamber) + 6.5 MW to upper divertor, ~ 22 MW overall.

Note that in the likely scenario of 18 poloidal limiters as part of the first wall the local flux will be enhanced over the values described above.

Appendix B: Particle fluxes and surface temperatures used for empirical scaling calculations

B. Lipschultz 20-6-2008

Technique: Used spreadsheets with data from the edge of the plasma edge and wall grids. They are from an equilibrium solution 1084 from A. Kukushkin. The profiles of fluxes and temperatures are shown in a series of figures following table 1.

Table 1 summarizes an effort to quantize sections of the divertor to be easily used in scaling calculations for T retention. The division into areas was made on the basis of the local ion flux density. For example the section 2 of the outer divertor was limited on both sides by the flux density dropping by a factor of 10 from the peak. The edge of section 3 was another factor of 10 lower in flux density still.

The surface temperatures were calculated for 2 cases – thermal conductivity kappa =150 W/m-K, and 50 W/m-K. The former covers an average conductivity (pan/pitch) for NB31 as well as for W. The latter is for neutron-damaged NB31.

Most variables plotted are self-explanatory. But Andre has given me the secret to the power loadings:

Wrad the radiation power;
Wpart the total power delivered with particles;
Wpls the total power delivered with charged particles (ions + electrons);
Wneu the total power delivered with neutrals;
Wheat the kinetic energy released at the target from impinging particles (ions + electrons + neutrals);
Wpot the potential energy released at the target from impinging particles (ions + electrons + neutrals).

The basic relations among these quantities are:
Wtot = Wrad + Wpart
Wpart = Wpls + Wneu = Wheat + Wpot

Please note that the kinetic energy delivered to the target is not equal to the product of the particle flux and the mean energy, since the kinetic energy of the reflected particles is subtracted. This is indeed the net power delivered to the target. You can use the difference between these two as a measure of the power reflected back from the surface.

One more comment to the same estimates: the electrons should also be included, they contribute 2*Te per electron (or 2*Z*Te per ion).

ITER High flux case

Outer divertor

total ion fluence = 1.56e24/s
total D fluence - 3e24/s
total power = 43 MW

2 thermal conductivities used
150 W/mK (for W and NB31)
50 W/mK (for neutron damaged NB31)

general atom flux 6.31313E+20 #/m2/s

Region	Area [m2]	T_surf_150	T_surf_50	Γatoms	E_atoms	Γions	E_ions	Γtotal	E_ave	Total ion flux	Total atom flux	Total flux
	m2	deg K	deg K	#/m2/s	eV	#/m2/s	eV	#/m2/s	eV	#/s	#/s	#/s
1	1.21	450	499	9.00E+22	1.5	6.00E+22	3	1.50E+23	2.1	7.26E+22	1.09E+23	1.82E+23
2	2.39	718	1305	1.10E+24	4.65	4.00E+23	9.8	1.50E+24	6.0	9.56E+23	2.63E+24	3.59E+24
3	7.67	645	1085	3.20E+22	29	6.10E+22	126	9.30E+22	92.6	4.68E+23	2.45E+23	7.13E+23
4	22.1	443	479	2.20E+21	33	3.00E+21	94	5.20E+21	68.2	6.63E+22	4.86E+22	1.15E+23

Inner divertor

total ion fluence = 1.1e24/s
total D fluence - 2.4e24/s
total power = 21.4 MW

5	1.15	447	492	3.30E+22	0.9	2.00E+22	1.9	5.30E+22	1.3	2.30E+22	3.80E+22	6.10E+22
6	4.4	591	925	4.80E+23	3.37	1.70E+23	7.5	6.50E+23	4.5	7.48E+23	2.11E+24	2.86E+24
7	4.9	507	675	3.90E+22	9	5.60E+22	20	9.50E+22	15.5	2.74E+23	1.91E+23	4.66E+23
8	6.1	449	495	3.20E+21	11.2	5.80E+21	25	9.00E+21	20.1	3.54E+22	1.95E+22	5.49E+22

Dome

total ion fluence - small
total atom fluence = 1.8e24/s
E_atom = 1.4 eV
Atom flux density = 2.8e22/m2/s
total power = 20 MW
area = 62 m2

9	62	447	490	2.80E+22	1.4	0.00E+00	0	2.80E+22	1.4	0.00E+00	1.74E+24	1.74E+24

Wall - limiter peaks (high flux)

Area 50 m2 half inner wall, half outer wall
ion flux =4.4e21/m2/s
Ion energy = 70-100eV
atom flux = 4.11e21
atom energy = 20 eV
ELM ion flux 2.2e21/m2/s
ELM ion energy 200 eV
T_surf 525 K

						ELM flux	ELM en	Ion flux	ion ener	total ion flux	avg ion energy	
						#/m2/s	eV	#/m2/s	eV	#/m2/s	eV	
						2.20E+21	200	4.40E+21	100	6.60E+21	133.3	
							Average ion energy (ELMs included) = 180 eV					
							Ion fluxes (ELMs + 'normal') combined					
10	50	440	475	3.93E+21	20	6.60E+21	133	1.05E+22	90.8	3.30E+23	1.97E+23	5.27E+23

Region	Area [m2]	T_surf_150	T_surf_50	Γatoms	E_atoms	Γions	E_ions	Γtotal	E_ave	Total ion flux	Total atom flux	Total flux
	m2	deg K	deg K	#/m2/s	eV	#/m2/s	eV	#/m2/s	eV	#/s	#/s	#/s
	Wall - between limiters (low flux region)											
	Area	315m2										
	ion flux	1e21/m2/s										
	ion energy	75 eV										
	Atom flux	1.31E+21										
	atom energ	20 eV										
	T_surf	450K										
11	**315**	**425**	**430**	**1.13E+21**	**20**	**1.00E+21**	**75**	**2.13E+21**	**45.8**	**3.15E+23**	**3.56E+23**	**6.71E+23**
	Wall - between limiters (shadowed regions)											
	Area	215 m2										
	ion flux	3e19/m2/s										
	ion energy	75 eV										
	atom flux	8.3e20/m2/s										
	atom energ	20 eV										
	T_surf	425K										
12	**215**	**425**	**425**	**6.46E+20**	**20**	**3.00E+19**	**75**	**6.76E+20**	**22.4**	**6.45E+21**	**1.39E+23**	**1.45E+23**
	Wall - only atom flux in completely shadowed areas											
	Area	177 m2										
	atom flux	8.3e20/m2/s										
	atom energ	20 eV										
	T_surf	425K										
13	**177**	**425**	**425**	**6.31E+20**	**20**	**0.00E+00**	**0**	**6.31E+20**	**20.0**	**0.00E+00**	**1.12E+23**	**1.12E+23**
	Upper divertor											
	Area	35 m2				#/m2/s	eV	#/m2/s	eV	#/m2/s	eV	
	steady state ion flux		9.4e21/m2/s			5.60E+20	200	9.40E+21	100	9.96E+21	105.6	
	ion energy		70-100 eV				**Average ion energy (ELMs included) = 180 eV**					
	atom flux		5.8e21/m2/s				**Ion fluxes (ELMs + 'normal') combined**					
	atom energy		20 eV									
	T_surf		475K for Kappa=150 W/mK, 565 for 50 W/mK									
	ELM time-averaged flu		5.6e20/m2/s			**Average ion energy (ELMs included) = 150 eV**						
	ELM energy		1000 eV									
14	**35**	**475**	**565**	**5.63E+21**	**20**	**1.00E+22**	**106**	**1.56E+22**	**75.0**	**3.50E+23**	**1.97E+23**	**5.47E+23**
							Total	**Main chamber**		**Ions (#/s)**	**Atoms (#/s)**	**atoms+ions**
										1.00E+24	**1.00E+24**	**2.00E+24**

Outer divertor

Various profiles are given below. Note that the sections shown in fig. 1 correspond to [-.045, .01], [.01, .065], [.065, .3], and [.3, 0.9].

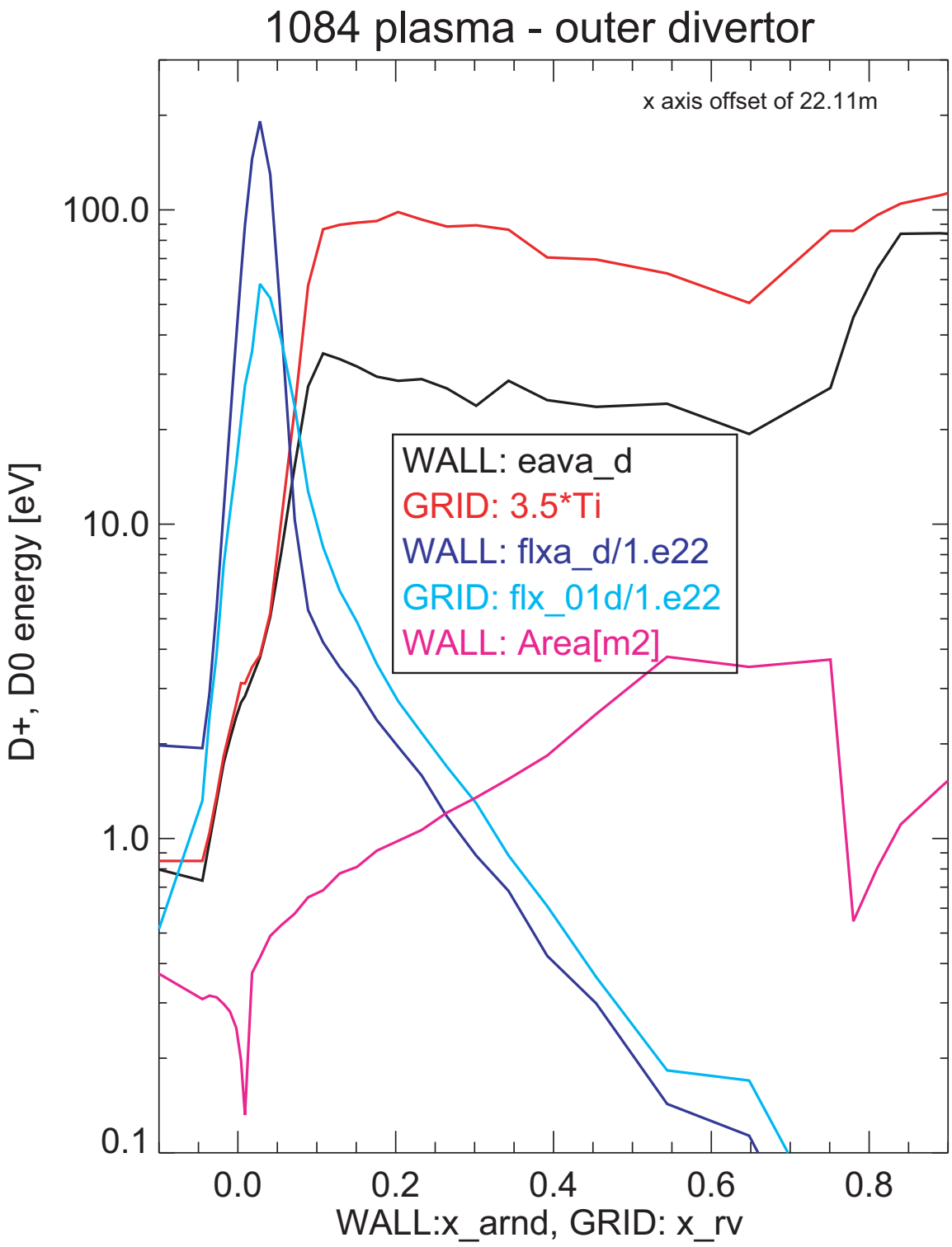

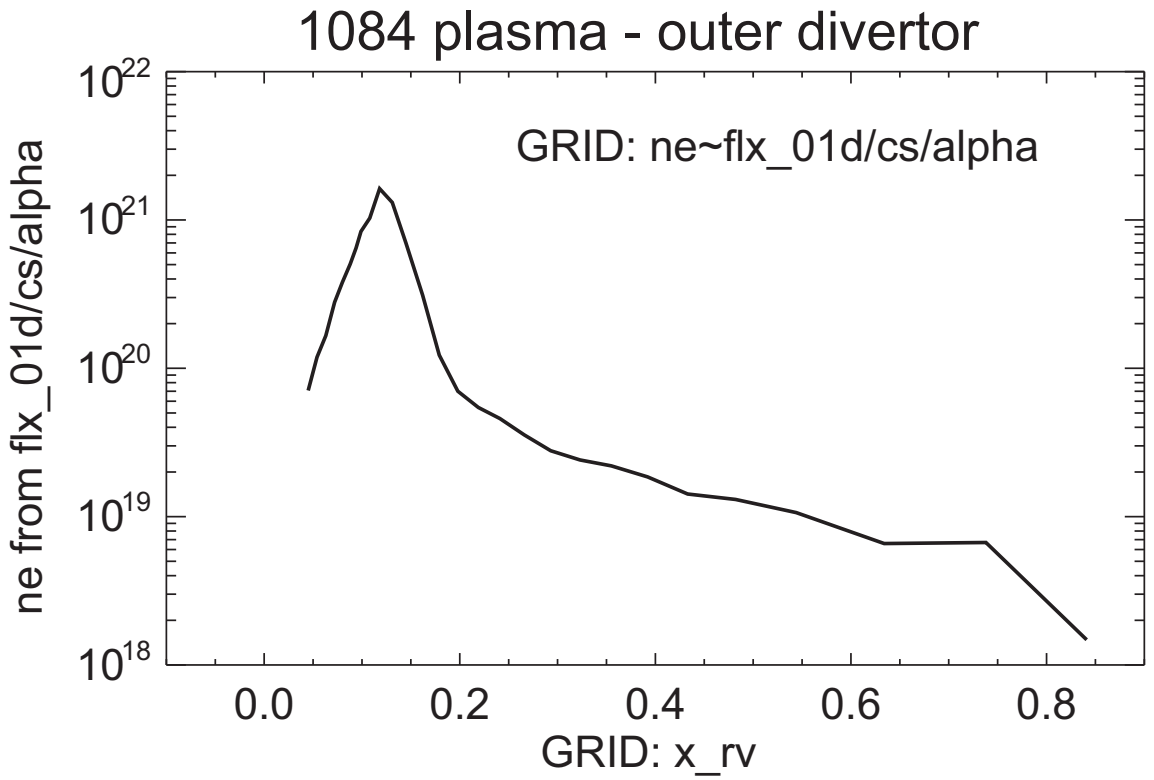
1084 plasma - outer divertor
GRID: ne~flx_01d/cs/alpha
ne from flx_01d/cs/alpha
10^{22}
10^{21}
10^{20}
10^{19}
10^{18}
0.0
0.2
0.4
0.6
0.8
GRID: x_rv

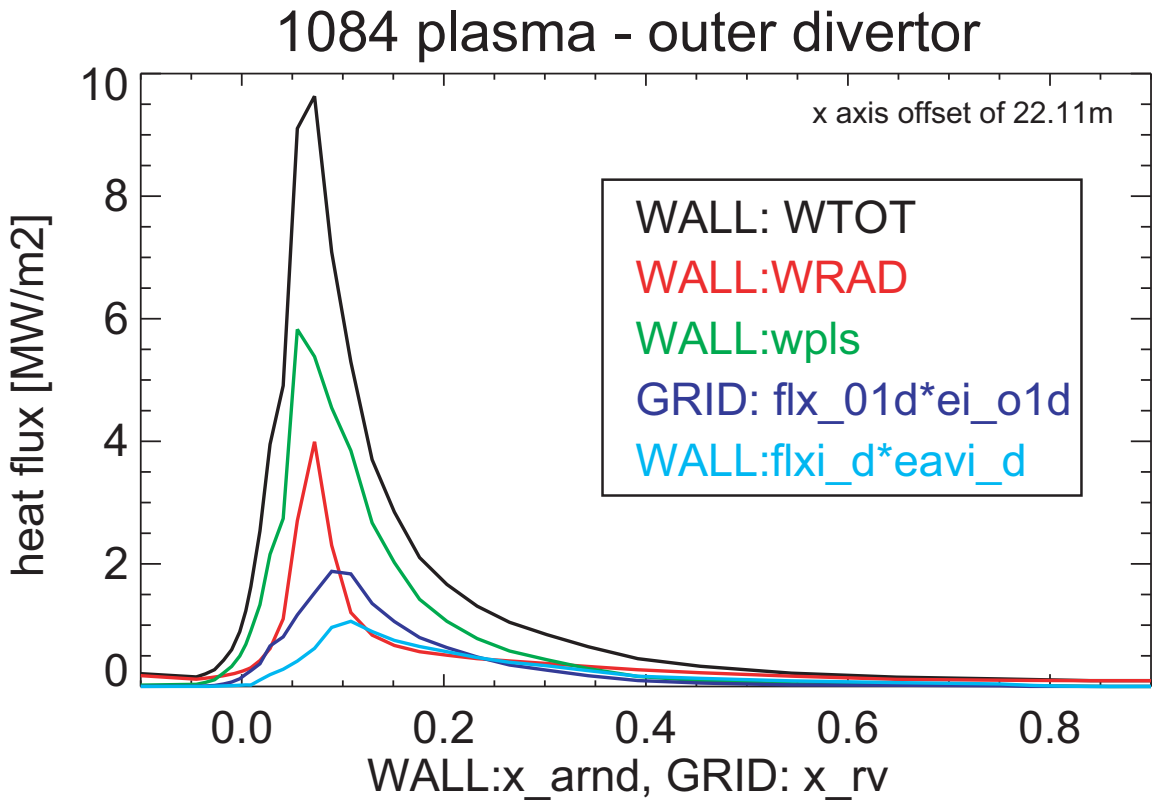
1084 plasma - outer divertor
x axis offset of 22.11m
WALL: WTOT
WALL:WRAD
WALL:wpls
GRID: flx_01d*ei_o1d
WALL:flxi_d*eavi_d
heat flux [MW/m2]
10
8
6
4
2
0
0.0
0.2
0.4
0.6
0.8
WALL:x_arnd, GRID: x_rv

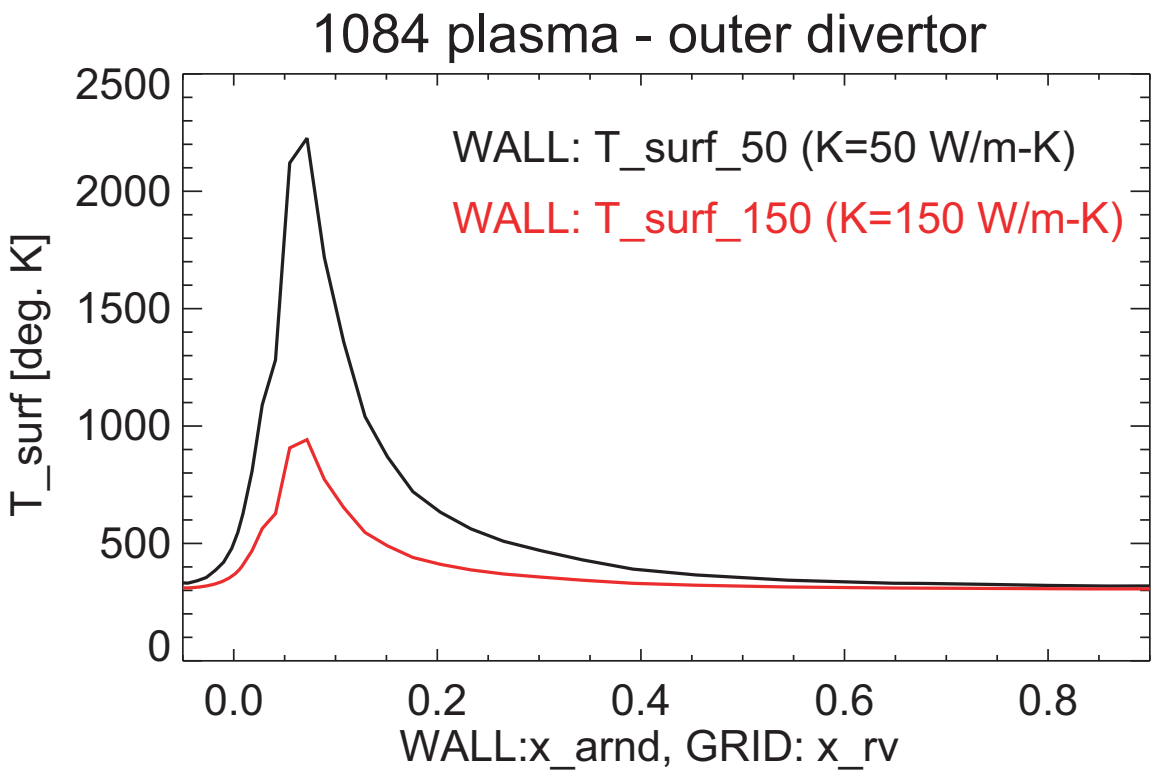
1084 plasma - outer divertor
WALL: T_surf_50 (K=50 W/m-K)
WALL: T_surf_150 (K=150 W/m-K)
T_surf [deg. K]
2500
2000
1500
1000
500
0
0.0
0.2
0.4
0.6
0.8
WALL:x_arnd, GRID: x_rv

Inner divertor: Various profiles are given below. Note that the sections shown in fig. 1 correspond to [-.05, .01], [.01, .17], [.17, .35], and [.35, 0.6].

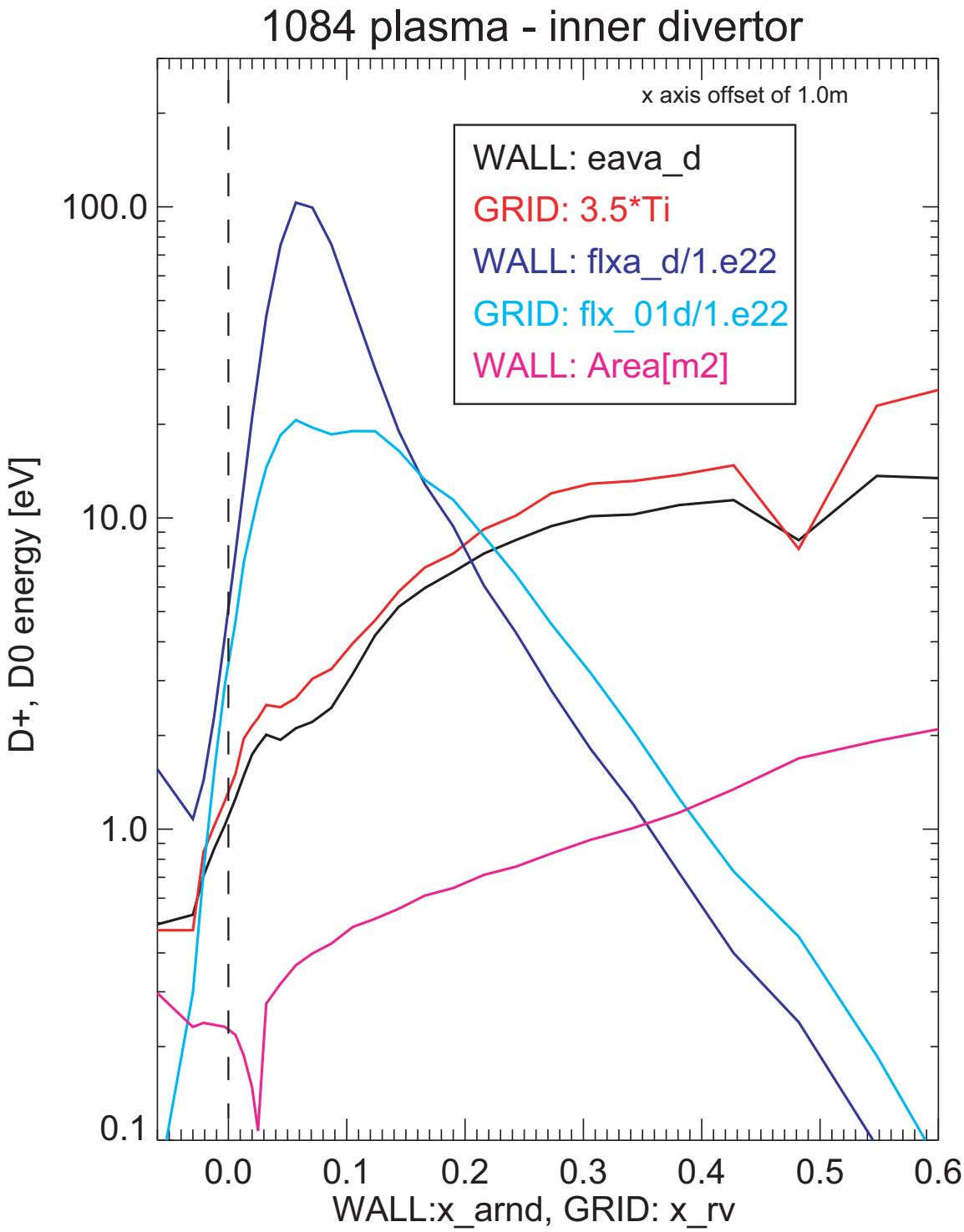

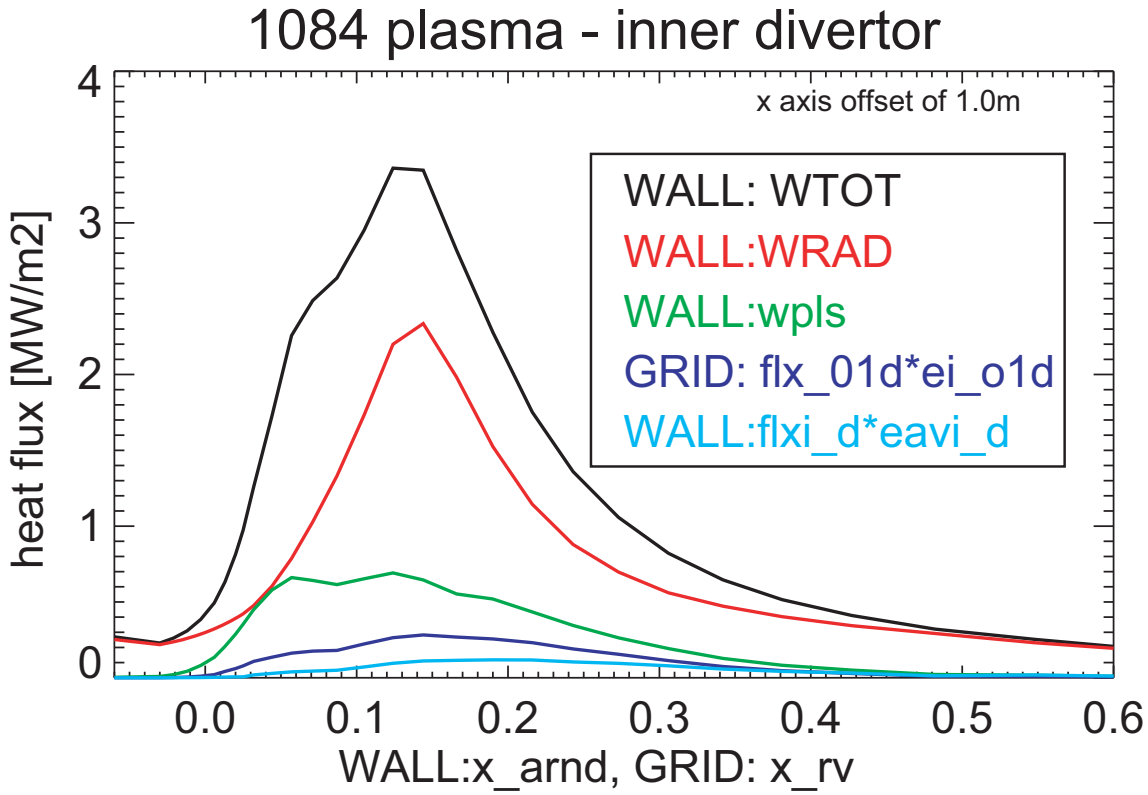
1084 plasma - inner divertor
x axis offset of 1.0m
WALL: WTOT
WALL:WRAD
WALL:wpls
GRID: flx_01d*ei_o1d
WALL:flxi_d*eavi_d
heat flux [MW/m2]
0
1
2
3
4
0.0
0.1
0.2
0.3
0.4
0.5
0.6
WALL:x_arnd, GRID: x_rv

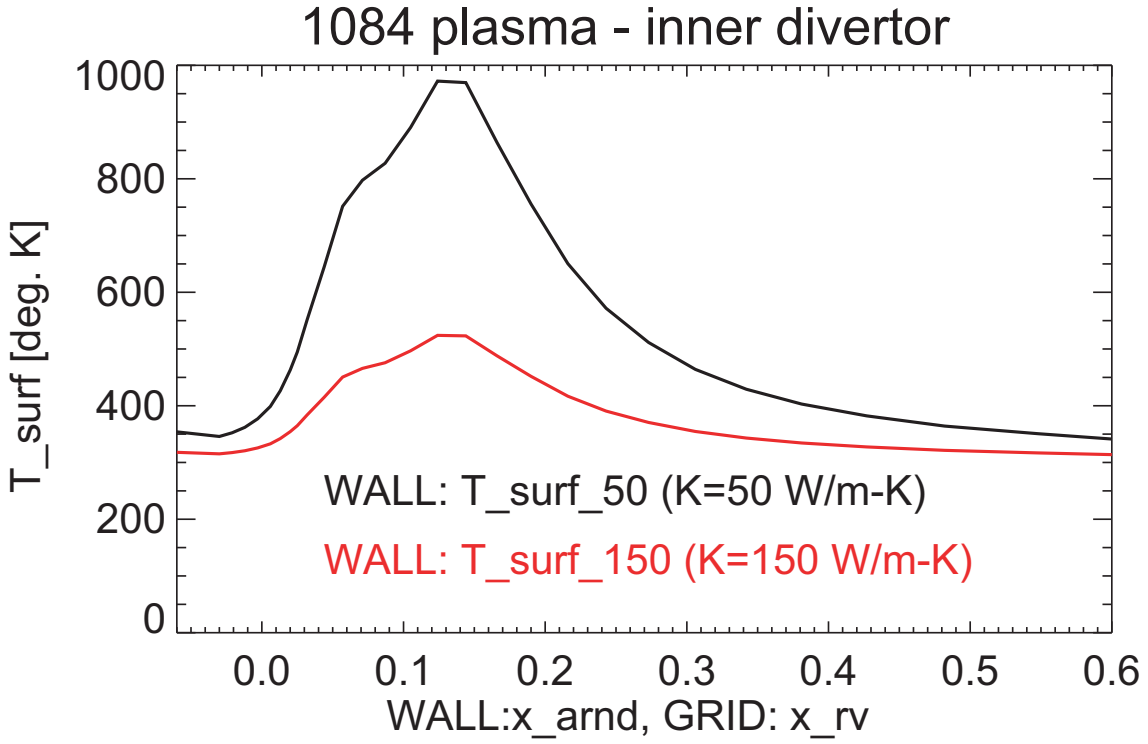
1084 plasma - inner divertor
T_surf [deg. K]
0
200
400
600
800
1000
WALL: T_surf_50 (K=50 W/m-K)
WALL: T_surf_150 (K=150 W/m-K)
0.0
0.1
0.2
0.3
0.4
0.5
0.6
WALL:x_arnd, GRID: x_rv

Dome:

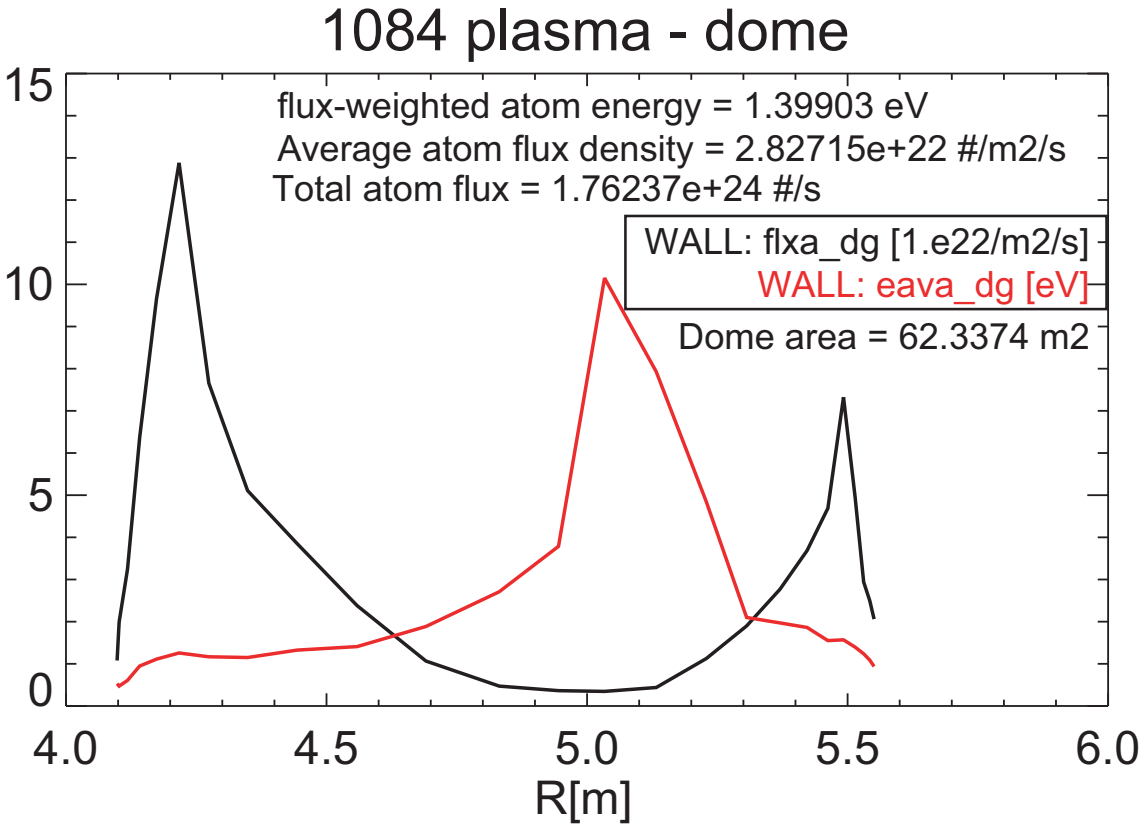
1084 plasma - dome
flux-weighted atom energy = 1.39903 eV
Average atom flux density = 2.82715e+22 #/m2/s
Total atom flux = 1.76237e+24 #/s
WALL: flxa_dg [1.e22/m2/s]
WALL: eava_dg [eV]
Dome area = 62.3374 m2
15
10
5
0
4.0
4.5
5.0
5.5
6.0
R[m]

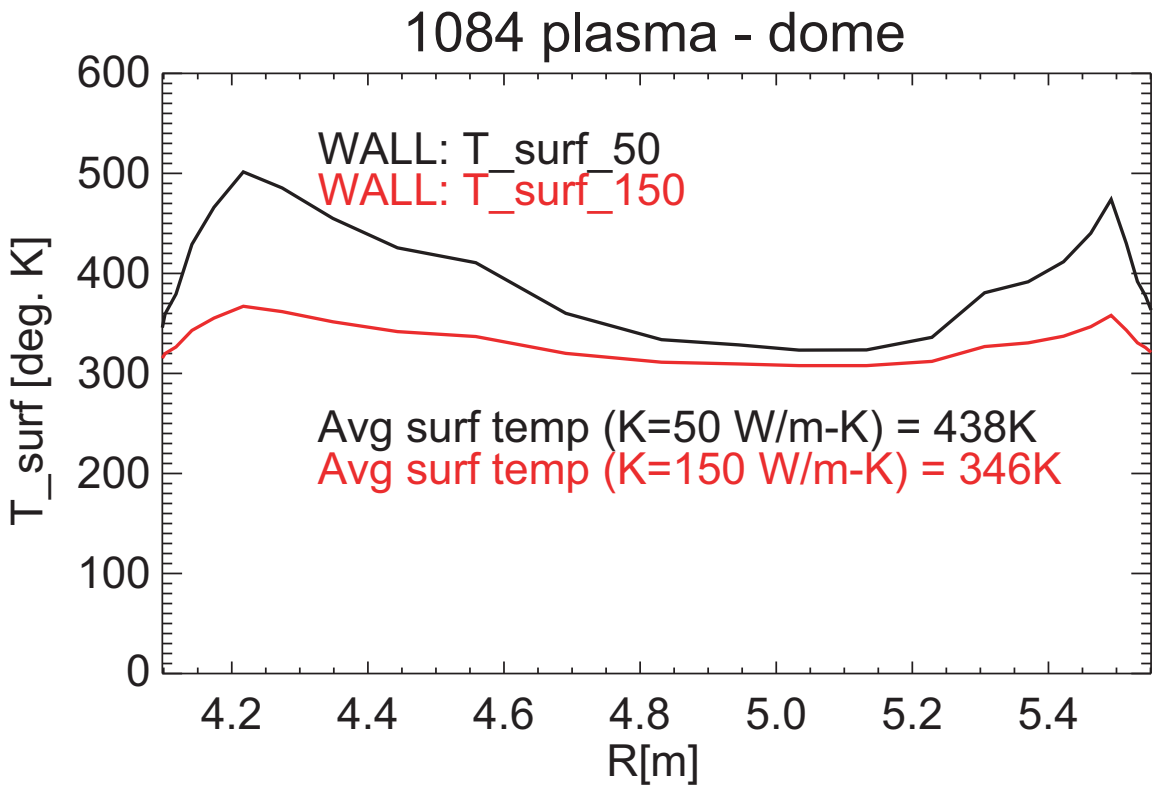
1084 plasma - dome
WALL: T_surf_50
WALL: T_surf_150
Avg surf temp (K=50 W/m-K) = 438K
Avg surf temp (K=150 W/m-K) = 346K
T_surf [deg. K]
600
500
400
300
200
100
0
4.2
4.4
4.6
4.8
5.0
5.2
5.4
R[m]

Appendix C – Comparison of available T diffusion and trapping codes (written by D. Whyte, June 20, 2008)

This writeup compares the two cases that Rob K. ran with TMAP/DIFFUSE for the benchmark. Data are tabulated in the Excel file also attached. I now include Olga's result after clarification of the total fluence / exposure time. These were for the "MIT" benchmark case at 2e23 D/m2/s. I have translated her results into g-T/m2 assuming 50:50 D:T.

Benchmark conditions for all my runs: constant T throughout PFC, 2 cm thick PFC, Frauenfelder diffusivity, bounce frequency in trap 1e13 /s. I have organized the data to g-T / m2 versus shot, assuming 50:50 D-T hydrogenic mix throughout.

The first comparison is for the "BPO report" benchmark, which is good to look at since DIFFUSE runs were also available. Case: fixed trap density ~0.65% W density, 1.4 eV traps, 2 nm implantation depth. Results are plotted for different incident flux and T below.

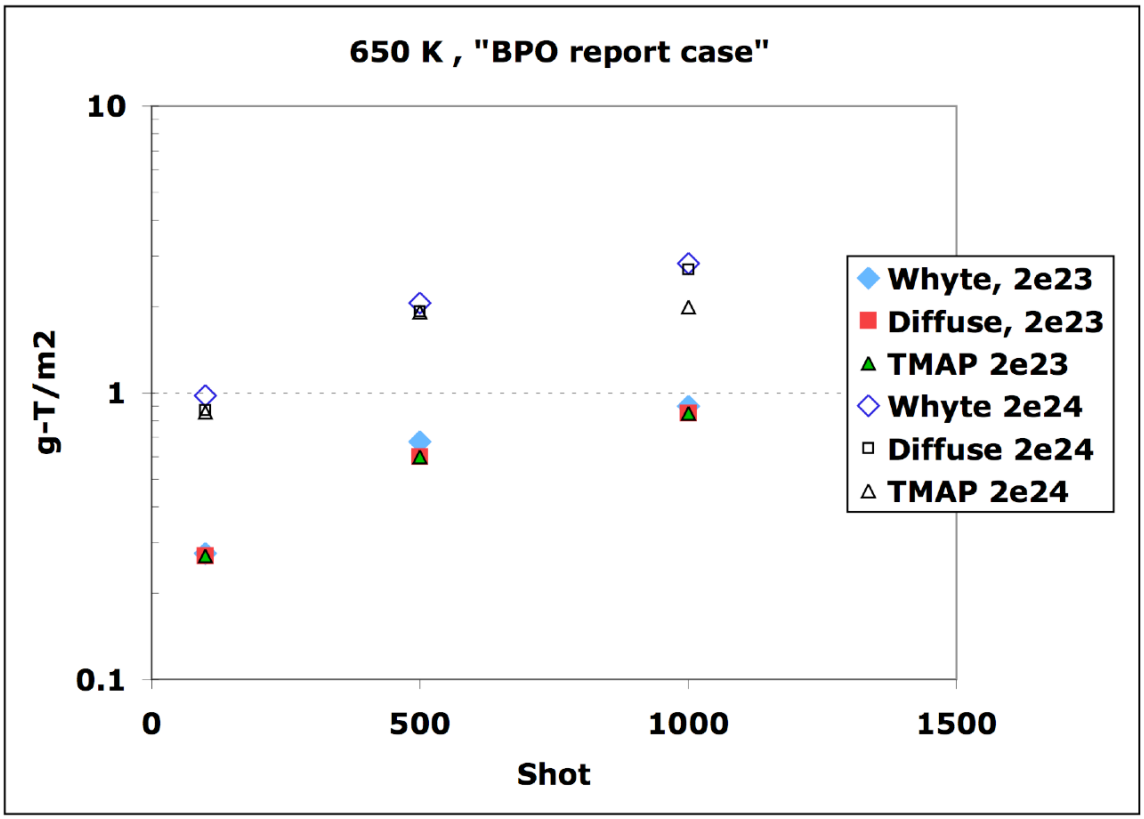

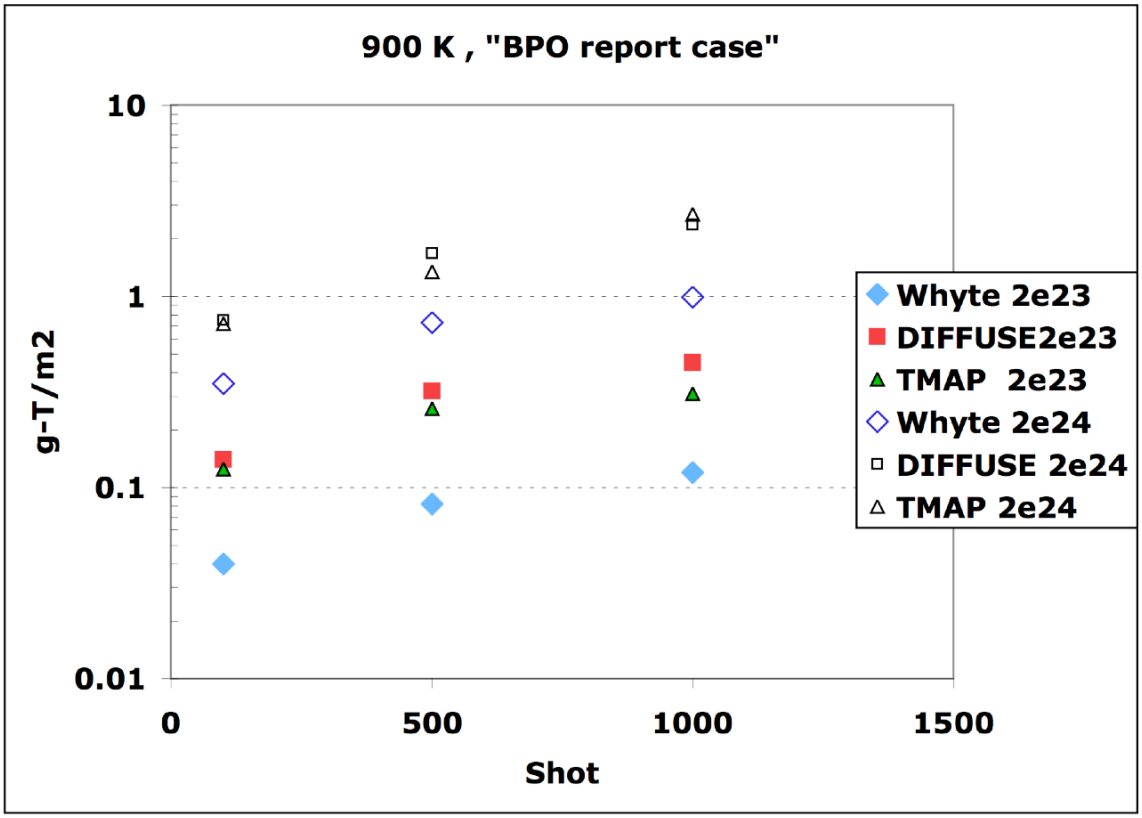

The agreement is very good between the three codes at 650 K in both absolute magnitude and trends versus shot and incident flux. At 900 K the codes diverge somewhat (factors up to three) in absolute levels, although the trend versus shot still look the same. My code calculation is on the lower side of TMAP/DIFFUSE. From my code I can see that the large reduction between the 650 K to 900 K case is the effect of de-trapping turning on, namely the quasi-equilibrium condition is that the traps are only partially filled (~2-10%) even though the solute H has permeated quite deeply. I checked the numerical results against a simple analytic model I have to calculate the equilibrium fraction of filled traps and they agree. Based on examining the analytic solution, it looks 900 K is just when (for these conditions) the de-trapping starts to turn on. Since the de-trapping is exponentially sensitive to T, it may be that a small detail in calculating the de-trapping rate is leading to the difference. In fact, my code uses the general formulation for de-trapping used in TMAP as below; so Rob and I could check details to spot the difference.

The form of trapping and de-trapping rate (/s) are taken from TMAP [60] as

$$R_{trap} = \frac{D n_{tr}}{\lambda^2 n_W} \qquad R_{de-trap} = \nu \exp(\frac{-E_{tr}}{kT_{PFC}}) \qquad \text{Eq. 3}$$

where λ is the distance between *empty* traps ~ , ν~10^{13} s^{-1} is the bounce frequency of H in traps and E_{tr}~1.5 eV is the trap activation energy

Now I show the comparison for the “MIT benchmark” case between my code and TMAP. Case: fixed trap density ~0.1% W density, 1.5 eV traps, 10 nm implantation depth.

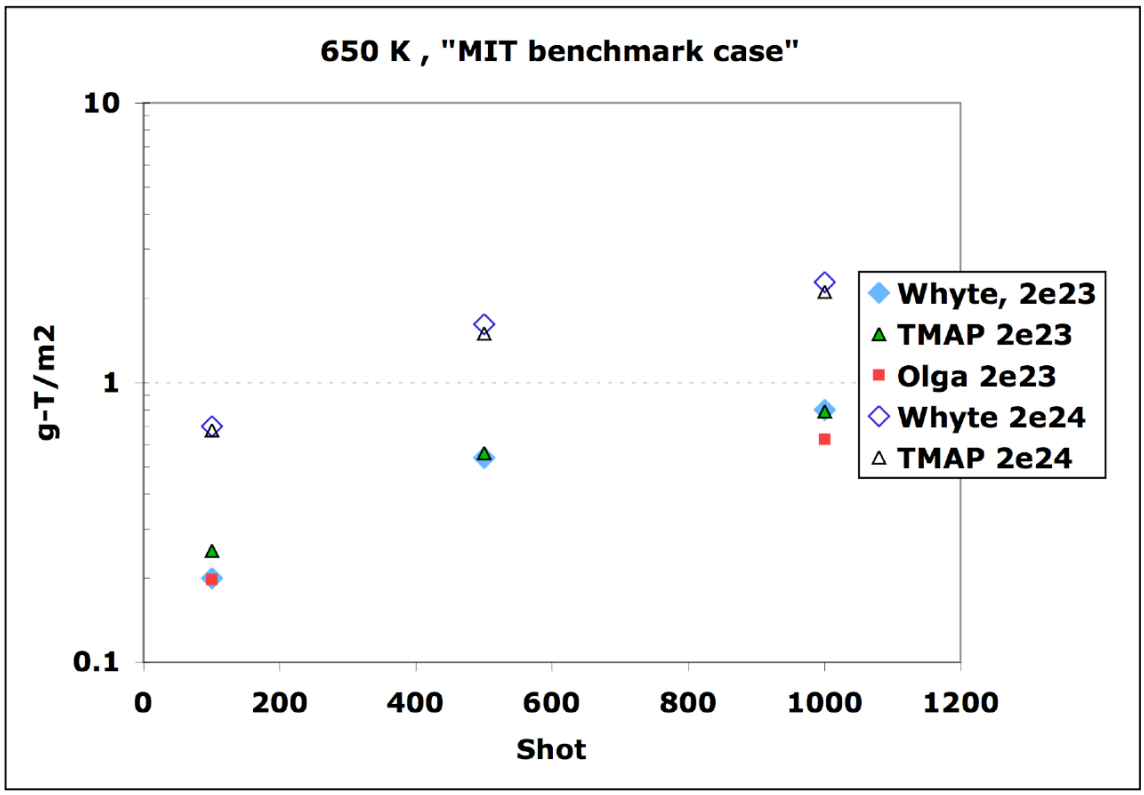

The three codes have excellent agreement for the 2e23 case versus shot number.

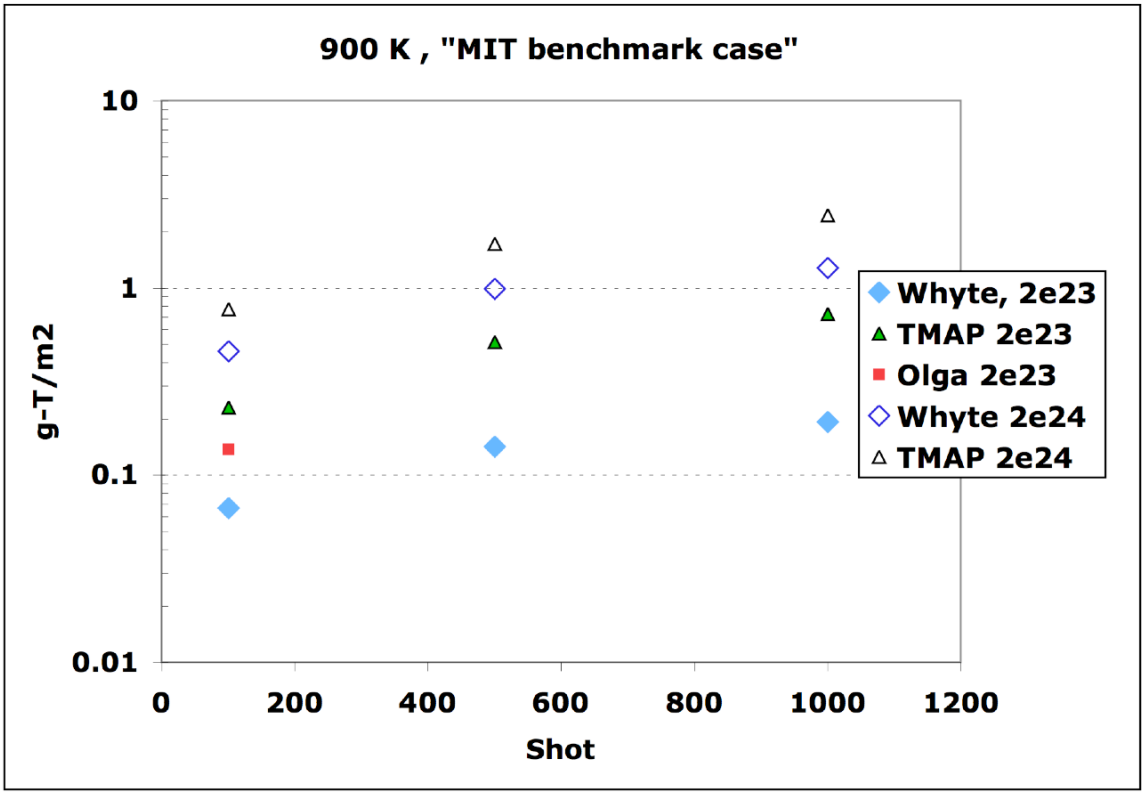

The agreement again is excellent at 600 K, but my calculation is factor 2-3 lower than TMAP at 900 K. Since this condition is not wildly different than the "BPO" case, I assume that the differences can be attributed to the same issues described above. Olga's result at 100 shots with 2e23 at 900K fall between TMAP and my calculation. The codes agree within a factor of three for the reduction in retention versus T. Since we all get the same answer at low T, I'd assume we're treating the permeation the same, and so these differences are due to different ways of handling de-trapping.

Appendix D: Comparison of TMAP and WW diffusion codes **(D. Whyte ca. Oct. 2008)**:

Before getting to the specific comparison between TMAP and WW, I'll note that my suspicion about the large slab thickness for my initial runs affecting the accuracy at this time scale are correct. For Case 3 I plot the trapped T density as a function of time (out to 1e5 s) for two cases with different slab thickness. Each line, starting from the top, represents a slab, moving into the material as one moves vertically down the plot.

For the case of 500 micron slabs we have for WW:

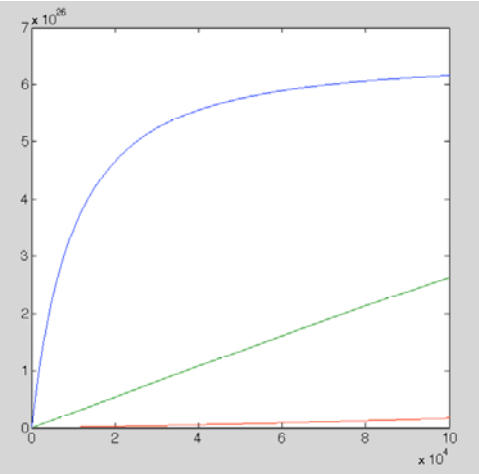

while for the case of 100 micron slabs we find:

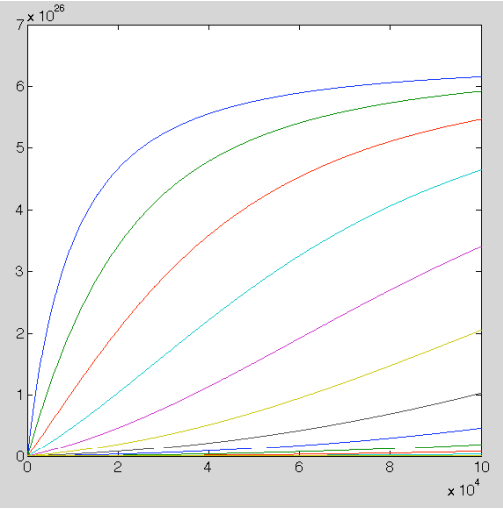

Evidently in the 500 micron slab case the T accounting accuracy is affected by the discrete slabs being too large in comparison to the diffusion depth at 1e5 s. This accuracy problem is resolved of course at longer times, as for example from the initial WW runs I replot the trapped T density, but now with the time axis out to 4e6 s.

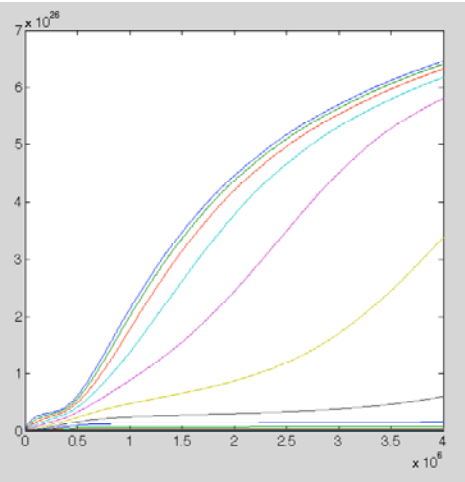

Now let's compare the WW runs with inputs matched to TMAP runs

a) Use 1/sqrt(3) correction to Frauenfelder for T
b) Fix trap solid fraction at 1e-2.
c) Have finer time resolution (10s → 1s) which will allow me to run the code with finer slab resolution if desired (as above)
d) Back T = 425 K

Other inputs kept the same such as surface T (WW uses T gradient as TMAP), flux, etc. These are for case with implantation only affecting C_{ss} so that recombination → infinity. I record two WW outputs for the different slab thicknesses in the model of 500 and 100 microns.

Case 3: Flux: 9.3e22 /m2/s, T_surf = 645 K, E_ions = 93 eV.

	Theory	**TMAP**	**WW: 500 micron**	**WW: 100 micron**
I (10^4 s) (m^{-2})	1.03E+23	1.02E+23	1.88e23	7.46e+22
I (10^5 s) (m^{-2})	3.27E+23	3.21E+23	4.48E+23	2.947E+23

Case 6: Flux: 6.5e23 /m2/s, T_surf = 591 K, E_ions = 4.5 eV.

	Theory	**TMAP**	**WW: 500 micron**	**WW: 100 micron**
I (10^4 s) (m^{-2})	6.05E+22	7.56E+22	8.96e22	3.13e+22
I (10^5 s) (m^{-2})	1.91E+23	2.37E+23	3.28+23	1.70E+23

Case 11: Flux: 2.1e21 /m2/s, T_surf = 425 K, E_ions = 46 eV.

	Theory	**TMAP**	**WW: 500 micron slab**	**WW: 100 micron slab**	**WW: 100 micron, x10 time-split**
I (10^4 s) (m^{-2})	1.10E+22	1.04E+22	3.78e21	1.19e+21	7.6e21
I (10^5 s) (m^{-2})	3.49E+22	3.18E+22	3.5+22	1.21E+22	4.56e22

At this point the conclusion is that the comparisons from theory, TMAP and WW are sufficiently good for cases 3 and 6, with the stipulation that WW is used with finer slab resolution for comparison at this relatively short time of 1e5 s.

The agreement for case 11 (the lowest flux case) is not so good, with in fact the disagreement becoming larger for finer grid resolution, which is the opposite of the expected trend. The reason for this underestimate by WW in case 11 is the time-splitting resolution I set in WW to keep the code numerically stable to trapping v. de-trapping, while accurately following diffusion processes on finer timescales (e.g. when heating is pulsed). This problem is easily detected in the trapped T density versus time for case 11 as in the table above, again with each line representing a slab in the model. The linear increase in time is the indicator that my time-splitting is too conservative for this particular case, i.e. even though the code has allowed diffusion of solute D to various layers the traps are effectively being filled at too slow a rate in the numerics, resulting in a linear increase in the trapped T density. As with the slab thickness, the limitation in accuracy imposed by the time-splitting vanishes at longer timescales. Note that the time-splitting can only ever underestimate the trapped T density if the numerics are stable.

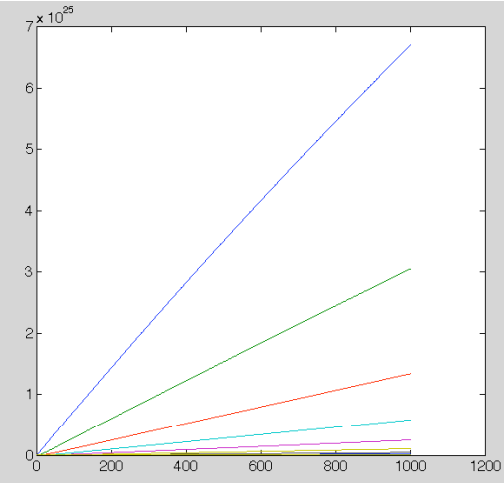

For comparison then at 1e5 s, I reduced the time-split, with the following result plotted below. Note that now the trapped T increases more like sqrt(time) which indicates my time-splitting is better suited to this case with reduced permeation.

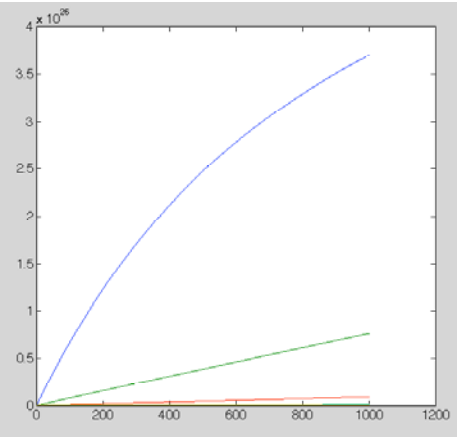

The results with the corrected time-split are also reported in the case 11 table. Note the much better agreement to TMAP, and that the WW result is slightly higher than TMAP, as expected from the slightly too coarse grid resolution at 100 microns.

Discussion

The conclusion is that WW is calculating the T retention to sufficient accuracy as compared to the analytic model and TMAP when the input parameters are kept consistent. The accuracy of these WW runs is in a sense intentionally poor at short timescales (< 1e4-1e5 s) since the goal was to examine deep permeation at long time-scales when the T inventory might approach the 700 g limit in ITER. The specific numerical inputs (larger slab thickness, conservative time-splitting) of these WW runs were geared toward that goal with the result that WW runs of this sort are very fast (< 5 minutes for all 14 ITER zones). Yet these WW runs provide further insight than the analytic model since it can accurately deal with the T gradient through the PFC and the time-evolving trap density. The numerical accuracy of the WW runs can/should be checked in each zone by simply plotting the T trap density versus time for each slab. The WW runs are sufficiently accurate at a particular time if: 1) the trapped tritium density is distributed through more than the top 1-2 slabs in the model and b) the trapped tritium density is not scaling exactly linearly in time which indicates that the time-splitting is too conservative.

References

[1]S. Ciattaglia, P Andrew, A. Loarte et al., in (Proc. of the 25th Symposium on Fusion Energy, Rostock, Germany, 2008), series, Vol., (2008) Paper P3.109.
[2]T. Loarer, C. Brosset, J. Bucalossi et al., Nuclear Fusion **47** (2007) 1112.
[3]J. N. Brooks, A. Kirschner, D. G. Whyte et al., Journal of Nuclear Materials **313-316** (2003) 424.
[4]J. Roth, A. Kirschner, W. Bohmeyer et al., Journal of Nuclear Materials **337-339** (2005) 970.
[5]A. Kirschner, D. Borodin, S. Droste et al., Journal of Nuclear Materials **363-365** (2007) 91.
[6]A.S. Kukushkin, H.D. Pacher, V. Kotov et al., Nuclear Fusion **45** (2005) 608.
[7]A. Kirschner, P. Wienhold, V. Philipps et al., Journal of Nuclear Materials **328** (2004) 62.
[8]Joachim Roth, Emmanuelle Tsitrone, Thierry Loarer et al., Plasma Physics and Controlled Fusion **50** (2008) 103001.
[9]A. A. Haasz, J. N. Brooks, R. Causey et al., "On US-BPO ITER task #5 - Choice of PFC for ITER," (University of Toronto Institute for Aerospace Studies (UTIAS), 2007).
[10]R. P. Doerner, A. Grossman, S. Luckhardt et al., Journal of Nuclear Materials **257** (1998) 51.
[11]H. Y. Guo, J. P. Coad, S. J. Davies et al., Journal of Nuclear Materials **241-243** (1997) 385.
[12]The JET Team, Journal of Nuclear Materials **176-177** (1990) 3.
[13]A. Kallenbach, R. Dux, J. Harhausen et al., Journal of Nuclear Materials **363-365** (2007) 60.
[14]A. Kreter, S. Brezinsek, J. P. Coad et al., Journal of Nuclear Materials **390-391** (2009) 38.
[15]M. Mayer, V. Rohde, K. Sugiyama et al., Journal of Nuclear Materials **390-391** (2009) 538.
[16]D.G. Whyte, J.P. Coad, P. Franzen, and H. Maier, Nuclear Fusion **39** (1999) 1025.
[17]Y. Gotoh, T. Tanabe, Y. Ishimoto et al., Journal of Nuclear Materials **357** (2006) 138.
[18]V. Philipps, 'Erosion-redeposition and fuel retention in JET C4-C15 campaigns', ITPA meeting report, November 6-9, 2006, Toronto.
[19]V. Philipps, 'JET conditioning with Beryllium', ITPA SOL/Divertor meeting report, January 9-12, 2006, Shanghai.
[20]M. Miyamoto, K. Tokunaga, T. Fujiwara et al., Journal of Nuclear Materials **313-316** (2003) 82.
[21]G. De Temmerman and R. P. Doerner, Journal of Nuclear Materials **389** (2009) 479.
[22]G. De Temmerman, M. J. Baldwin, R. P. Doerner et al., Journal of Nuclear Materials **390-391** (2009) 564.
[23]G. De Temmerman, M. J. Baldwin, R. P. Doerner et al., Nuclear Fusion **48** (2008) 075008.
[24]A. A. Haasz, J. W. Davis, M. Poon, and R. G. Macaulay-Newcombe, Journal of Nuclear Materials **258-263** (1998) 889.
[25]O. V. Ogorodnikova, J. Roth, and M. Mayer, Journal of Nuclear Materials **373** (2008) 254.
[26]R. Causey, K. Wilson, T. Venhaus, and W. R. Wampler, Journal of Nuclear Materials **266-269** (1999) 467.
[27]I. Alessandrini, G. Maddaluno, G. Giacomi, and W. Bohmeyer, 'Report on deuterium desorption from W-1% La2O3 samples after exposure in plasma generators', ENEA Frascati report FUS TN PF-TS-R-004, 2001,
[28]V.Kh. Alimov and J. Roth, Physica Scripta **T128** (2007) 6.
[29]G.M. Wright, "The dynamics of hydrogen retention in irradiated molybdenum," PhD, University of Wisconsin, 2007.
[30]R. Doerner (personal communication).
[31]V. Kh Alimov, W. M. Shu, J. Roth et al., Physica Scripta **in press** (2009).

[32]J. P. Sharpe, R. D. Kolasinski, M. Shimada et al., Journal of Nuclear Materials **390-391** (2009) 709.
[33]W. R. Wampler and R. Doerner, Physica Scripta**, in press** (2009).
[34]V. Philipps (personal communication).
[35]K. Sugiyama, M. Mayer, V. Rohde et al., Nuclear Fusion **submitted to** (2009).
[36]O. V. Ogorodnikova, J. Roth, and M. Mayer, Journal of Nuclear Materials **313-316** (2003) 469.
[37]V. Rohde, V. Mertens, and A. Scarabosio, Journal of Nuclear Materials **390-391** (2009) 474.
[38]B. Lipschultz, D. G. Whyte, J. Irby et al., Nuclear Fusion **49** (2009) 045009.
[39]K. Tokunaga, M. J. Baldwin, R. P. Doerner et al., Journal of Nuclear Materials **337-339** (2005) 887.
[40]G. N. Luo, W. M. Shu, and M. Nishi, Fusion Engineering and Design **81** (2006) 957.
[41]V. Kh Alimov, J. Roth, R. A. Causey et al., Journal of Nuclear Materials **375** (2008) 192.
[42]O. V. Ogorodnikova, J. Roth, and M. Mayer, Journal of Applied Physics **103** (2008) 034902.
[43]S. M. Myers, P. M. Richards, W. R. Wampler, and F. Besenbacher, Journal of Nuclear Materials **165** (1989) 9.
[44]"Evaluated Nuclear Data File," (National Nuclear Data Center, Brookhaven National Laboratory).
[45]H. Iida, V. Khripunov, V. Petrizzi, and G. Federici, 'ITER Nuclear Analysis Report', ITER report G 73 DDD 2 W 0.2, 2004,
[46]C. H. M. Broeders and A. Yu Konobeyev, Journal of Nuclear Materials **328** (2004) 197.
[47]H. Eleveld and A. van Veen, Journal of Nuclear Materials **212-215** (1994) 1421.
[48]M. Fukumoto, H. Kashiwagi, Y. Ohtsuka et al., Journal of Nuclear Materials **390-391** (2009) 572.
[49]W. R. Wampler and R. P. Doerner, Nuclear Fusion **49** (2009) 115023.
[50]I. Takagi, S. Watanabe, S. Nagaoka, and K. Higashi, Fusion Science and Technology **41** (2002) 897.
[51]G. M. Wright, D. G. Whyte, and B. Lipschultz, Journal of Nuclear Materials **390-391** (2009) 544.
[52]J.F. Ziegler, J.P. Biersack, and U. Littmark, "SRIM," in The Stopping and Range of Ions in Solids (Pergamon Press, New York, 1985).
[53]P. Jung, "1.5 Production of atomic defects in metals in thermal equilibrium," in Atomic Defects in Metals, edited by H. Ullmaier (Springer Verlag, 1991), Vol. 25, pp. 4-5.
[54]W. M. Shu, M. Nakamichi, V. Kh Alimov et al., Journal of Nuclear Materials **390-391** (2009) 1017.
[55]G. Federici, C.H. Skinner, J.N. Brooks et al., Nuclear Fusion **41** (2001) 1967.
[56]M. A. Pick and K. Sonnenberg, Journal of Nuclear Materials **131** (1985) 208.
[57]R.A. Anderl, D.F. Holland, G.R. Longhurst et al., Fusion Technology **21** (1992) 745.
[58]W. R. Wampler, Journal of Nuclear Materials **145-147** (1987) 313.
[59]P. Franzen, C. Garcia-Rosales, H. Plank, and V. Kh Alimov, Journal of Nuclear Materials **241-243** (1997) 1082.
[60]G.R. Longhurst, 'TMAP-7 user Manual', Idaho National Laboratory report INEEL/EXT-04-02352, 2004,
[61]D. G. Whyte, Journal of Nuclear Materials **390-391** (2009) 911.
[62]K. Schmid, Nuclear Fusion **48** (2008) 105004.
[63]A. Kirschner, D. Borodin, V. Philipps et al., Journal of Nuclear Materials **390-391** (2009) 152.
[64]J. Roth, R. Preuss, W. Bohmeyer et al., Nuclear Fusion **44** (2004) L21.

[65]G. Federici, P. Andrew, P. Barabaschi et al., Journal of Nuclear Materials **313-316** (2003) 11.
[66]V. Kh Alimov, W. M. Shu, J. Roth et al., 'Deuterium retention in tungsten exposed to pure and helium-seeded deuterium plasmas', ITPA SOL/Divertor report, January 9-12, 2009, Amsterdam.
[67]S. Lindig, M. Balden, V. Kh Alimov et al., Physica Scripta **in press** (2009).
[68]J. Roth, S. Lindig, M. Balden et al., 'Correlation of sub-surface structural changes with hydrogen concentrations in Tungsten', ITPA SOL/Divertor report, January 9-12, 2009, Amsterdam.
[69]M. Mayer, 'Deuterium permeation through W foils - diffusivity and trap concentration', ITPA SOL/Divertor report, January 9-12, 2009, Amsterdam.
[70]M. I. Baskes, Journal of Nuclear Materials **92** (1980) 318.
[71]Z. Tian, J.W. Davis, and A. A. Haasz, Journal of Nuclear Materials **in press** (2009).
[72]Y. Ueda, M. Fukumoto, Y. Ohtsuka et al., 'D behavior in damaged W by high energy ion beam', ITPA SOL/Divertor report, September 15-18, 2008, Nagasaki.
[73]B. Tyburska, V. Kh Alimov, O. V. Ogorodnikova et al., Journal of Nuclear Materials **In Press** (2009).
[74]W. R. Wampler and R. Doerner, 'Retention of deuterium at displacement damage in plasma-exposed tungsten', ITPA SOL/Divertor report, January 9-12, 2009, Amsterdam.
[75]R. Doerner, 'Simultaneous D/He implantation in W using PISCES', ITPA SOL/Divertor report, January 9-12, 2009, Amsterdam.
[76]H.T. Lee, A. A. Haasz, and J. W. Davis, Journal of Nuclear Materials **363-365** (2007) 898.
[77]Y. Ueda, M. Fukumoto, J. Yoshida et al., Journal of Nuclear Materials **386-388** (2009) 725.
[78]Y. Ueda, S. Kajita, N. Ohno et al., 'Formation condition of nano-structure and retention/blistering under He/D plasma', ITPA SOL/Divertor report, January 9-12, 2009, Amsterdam.
[79]Y. Ueda, H. Kashiwagi, M. Fukumoto et al., Fusion Science and Technology **56** (2009) 85.
[80]A. Kallenbach, N. Asakura, A. Kirk et al., Journal of Nuclear Materials **337-339** (2005) 381.
[81]A.S. Kukushkin, H.D. Pacher, G.W. Pacher et al., Nuclear Fusion **43** (2003) 716.
[82]A. Kallenbach, M.N.A. Beurskens, A. Korotkov et al., Nuclear Fusion **42** (2002) 1184.
[83]B. Lipschultz, P. Andrew, J. Coad et al., in (Proc. of the 30th European Conf. On Controlled Fusion and Plasma Physics, St. Petersburg, Russia, 2003), series, Vol., European Physical Society, Geneva (2003).
[84]B. Lipschultz, D. Whyte, and B. LaBombard, Plasma Phy. & Cont. Fusion **47** (2005) 1559.
[85]A. W. Leonard, J. A. Boedo, M. Groth et al., Journal of Nuclear Materials **363-365** (2007) 1066.